https://doi.org/10.5194/egusphere-2025-5277
Preprint. Discussion started: 18 November 2025

Contrasting Impacts of Dust Ice-Nucleating Particles on the Evolution and Radiative Effects of Mixed-Phase and Ice Clouds

Hua Zhang[1,2], Shuxiao Wang[1,2], Xi Zhao[3], Zhijun Wu[4,5], Yan Yin[6], Siyu Chen[7], Dantong Liu[8], Jingchuan Chen[4], Hui Jiang[6], Jiewen Shen[1,2], Da Gao[1,2], Dejia Yin[1,2], Yicong He[1,2], Zeqi Li[1,2], Shengyue Li[1,2], Zhaoxin Dong[9], Manish Shrivastava[10], and Bin Zhao[1,2]

[1]State Key Laboratory of Regional Environment and Sustainability, School of Environment, Tsinghua University, Beijing, 100084, China
[2]State Environmental Protection Key Laboratory of Sources and Control of Air Pollution Complex, Beijing, 100084, China
[3]Institute of Surface-Earth System Science, School of Earth System Science, Tianjin University, Tianjin, 300072, China
[4]State Key Laboratory of Regional Environment and Sustainability, College of Environmental Sciences and Engineering, Peking University, Beijing, 100871, China
[5]Collaborative Innovation Center of Atmospheric Environment and Equipment Technology, Nanjing University of Information Science and Technology, Nanjing, 210044, China
[6]KNMI-NUIST Center for Atmospheric Composition, Nanjing University of Information Science and Technology, Nanjing, 210044, China
[7]Key Laboratory for Semi-Arid Climate Change of the Ministry of Education, Lanzhou University, Lanzhou, 730000, China
[8]Department of Atmospheric Sciences, School of Earth Sciences, Zhejiang University, Hangzhou, 310058, China
[9]School of Environment and Energy, South China University of Technology, Guangzhou Higher Education Mega Center, Guangzhou, 510006, China
[10]Pacific Northwest National Laboratory, Richland, Washington, 99352, USA

Correspondence: Bin Zhao (bzhao@mail.tsinghua.edu.cn)

https://doi.org/10.5194/egusphere-2025-5277
Preprint. Discussion started: 18 November 2025

Abstract

The effect of aerosols acting as ice-nucleating particles (INPs) remains one of the least understood processes in aerosol–cloud–climate interactions. Mineral dust can serve as INPs in both mixed-phase and ice clouds, yet few studies have simultaneously considered dust INPs in both cloud types, limiting our understanding of their impacts on clouds and radiation. Here, we develop an improved INP parameterization in WRF-Chem that explicitly represents dust INPs in both cloud types, incorporating both non-size-resolved and size-resolved INP parameterizations. Model evaluation against ground-based and satellite observations shows good agreement with the observed spatiotemporal variations of surface PM_{10}, dust INPs, liquid water path (LWP), and ice water path (IWP) over East Asia. Simulations for spring 2018 reveal that dust INPs in mixed-phase clouds accelerate the Wegener–Bergeron–Findeisen (WBF) process, increasing IWP by 2.3% and decreasing LWP by 3.3%, thereby reducing cloud albedo and producing a warming of 0.20 W m^{-2}. In ice clouds, dust INPs enhance heterogeneous nucleation, increase ice crystal number concentrations, and reduce their effective radius. Sedimenting ice crystals from ice clouds further intensify the WBF process in mixed-phase clouds, ultimately yielding a stronger warming of 3.56 W m^{-2}. Differences among INP parameterizations are comparable to those between simulations with and without INPs, whereas the size-resolved scheme may more reasonably represent the spatial variability of dust INP effects. This study highlights the distinct roles of dust INPs in mixed-phase and ice clouds from the microphysical perspective and advances our understanding of aerosol–cloud–climate interactions.

1 Introduction

Ice-nucleating particles (INPs) play a crucial role in initiating ice crystal formation in the atmosphere, yet this process remains one of the least understood aspects of aerosol–cloud–climate interactions (Cantrell and Heymsfield, 2005; Gultepe and Heymsfield, 2016; Seinfeld et al., 2016). Ice crystals can form through homogeneous nucleation, which occurs when supercooled droplets or solutions freeze spontaneously below −37°C (Koop et al., 2000). They can also form through heterogeneous nucleation, in which INPs enable ice formation at higher temperature and lower supersaturation (DeMott et al., 2010; Kiselev et al., 2017; Bi et al., 2017; Knopf et al., 2018; Holden et al., 2019; Zhao et al., 2019). Understanding the sources, properties, and representation of INPs is therefore fundamental to improving cloud and climate simulations.

Mineral dust is widely recognized as the dominant atmospheric INP source, owing to both its high ice-forming efficiency (Murray et al., 2012; Chen et al., 2021; Burrows et al., 2022) and large emission loads (Textor et al., 2006). Dust can be activated as INP

https://doi.org/10.5194/egusphere-2025-5277
Preprint. Discussion started: 18 November 2025

in both mixed-phase clouds, which contain liquid droplets and ice crystals (DeMott et al., 2015; Kanji et al., 2017), and ice clouds, which consist exclusively of ice crystals (Vali, 1985). Numerical modeling has been the primary approach to assessing their effects on clouds and radiation, but most studies rely on limited parameterization schemes that capture only part of the dust INP spectrum, either for mixed-phase or ice clouds, rarely both.

For mixed-phase clouds, most modeling studies have used simple empirical parameterization schemes to describe dust INP activation. These studies generally found that dust INPs accelerate the Wegener–Bergeron–Findeisen (WBF) process, which speeds up the conversion of liquid water to ice (Shi and Liu, 2019; Kawai et al., 2021; Shi et al., 2022; Luo et al., 2023; Liu et al., 2011). The result is usually a reduction in the liquid water path (LWP), a decrease in shortwave reflectivity, and an increase in longwave transmittance. However, the radiative response differs strongly across regions and seasons, as shown in Shi and Liu (2019) and Shi et al. (2022). These differences reflect a major limitation. Dust INPs in mixed-phase clouds have rarely been validated with observations, and parameterization schemes differ greatly in their treatment of dust size distributions and activation spectra. As a result, current understanding is highly uncertain, and systematic evaluation using multiple schemes is still needed.

For ice clouds, most studies have represented dust INPs with deposition nucleation or immersion freezing schemes that were designed for cirrus conditions. Using these approaches, Liu et al. (2012), Kuebbeler et al. (2014), and Beer et al. (2024) reported that dust INPs reduce the number of ice crystals and produce larger crystals compared to homogeneous freezing. This is often called the negative Twomey effect. It usually results in thinner cirrus clouds and a cooling effect. Event-based simulations also show similar behavior. For example, Weger et al. (2018) and Zeng et al. (2023) found that high dust concentrations during the April 2014 European dust outbreak and the May 2017 East Asian event enhanced deposition nucleation and reduced ice crystal size. Su and Fung (2018b) showed that dust increased ice water but slightly reduced liquid water over East Asia. These results are valuable, but they depend strongly on the INP parameterization used. Because most schemes treat only cirrus conditions, their results cannot be generalized to the full climate system.

In summary, existing modeling studies have usually examined either mixed-phase or ice clouds, but very few have treated both together. This separation is mainly because parameterization schemes were developed for only one type of cloud. As a result, the overall effects of dust INPs on clouds and radiation remain poorly understood. In this study, we developed a comprehensive dust INP parameterization that consistently represents both mixed-phase and ice-phase activation. The scheme also considers size-resolved dust properties and is evaluated against various observations, including INP concentrations. This allows us to perform a systematic assessment of dust INP effects across both cloud types. Our results provide a stronger basis for understanding aerosol–cloud–climate interactions and for improving climate prediction.

https://doi.org/10.5194/egusphere-2025-5277
Preprint. Discussion started: 18 November 2025

2 Methods

In this study, we developed an improved INP parameterization within version 4.2 of the Weather Research and Forecasting model coupled with Chemistry (WRF-Chem; Grell et al., 2005). The new scheme explicitly represents dust INPs in both mixed-phase and ice clouds, together with several modifications to the dust simulation, thereby providing a more comprehensive description of atmospheric INPs. Specifically, we (1) implemented the Shao2011 dust emission scheme (Shao et al., 2011) within the Model for Simulating Aerosol Interactions and Chemistry (MOSAIC) aerosol module (Zaveri et al., 2008) with 20 size bins, (2) introduced dust-aware INP parameterizations for mixed-phase and ice clouds, and (3) coupled the diagnosed dust INP concentrations to the Morrison two-moment microphysics scheme (Morrison et al., 2005). These developments directly affect the number concentrations and effective radius of cloud droplets and ice crystals, and further influence liquid water path (LWP), ice water path (IWP), and radiative balance.

2.1 Dust emission scheme

The Taklimakan Desert (TD) and the Gobi Desert (GD) are the two dominant dust source regions in East Asia (Sun et al., 2001; Zhang et al., 2008; Wang et al., 2012). Dust cycle is simulated using the Shao2011 dust emission scheme (Shao et al., 2011) in combination with the Zhang2001 dry deposition scheme (Zhang, 2001), following the evaluation of Zeng et al. (2020), who identified this configuration as optimal for East Asia.

The Shao2011 scheme calculates dust emission as a function of surface erodibility, vegetation fraction, soil particle size distribution, soil moisture, and near-surface winds (Shao et al., 2011). Specifically, the erodibility factor prescribes the fraction of erodible surface in each grid cell, and the vegetation fraction reduces the effective bare soil area exposed to wind erosion. The soil particle size distribution regulates the emitted dust mass across different size bins, while soil moisture suppresses dust emission by enhancing inter-particle cohesion. The erodibility distribution applied in this study is shown in Fig. S1.

In WRF-Chem, the Shao2011 scheme is originally implemented only within the Goddard Chemistry Aerosol Radiation and Transport (GOCART) aerosol module. Here, we established a new coupling by integrating Shao2011 with MOSAIC, which resolves 20 size bins (0.000968–10 μm). Moreover, as suggested by Zeng et al. (2020), we adopted the soil particle size distribution from WRF-Chem v3.7.1, as it yields dust simulations that are more consistent with observations compared with the default distribution in WRF-Chem v4.2.

It has been shown that the National Centers for Environmental Prediction Final Operational Global Analysis (NCEP/FNL) reanalysis data that drive the WRF-Chem model are biased towards high soil moisture, often resulting in unsatisfactory dust

https://doi.org/10.5194/egusphere-2025-5277
Preprint. Discussion started: 18 November 2025

simulations (Chen and Mitchell, 1999). To mitigate this problem, we employed the Climate Change Initiative soil moisture (CCIrec, 1989–2021) global long-term non-missing satellite soil moisture product developed by Hu et al. (2023), which avoids the overestimation of soil moisture inherent in the FNL reanalysis data.

2.2 Ice nucleation parameterizations

In the atmosphere, four major heterogeneous nucleation pathways are identified: deposition nucleation, immersion freezing, contact freezing, and condensation freezing (Kanji et al., 2017). Deposition nucleation refers to the direct deposition of water vapor onto the surface of INPs under ice-supersaturated conditions, in the absence of liquid droplets (Burrows et al., 2022). Immersion freezing occurs when INPs are first activated as cloud condensation nuclei to form droplets, which subsequently freeze upon further cooling (Kanji et al., 2017). Contact freezing, by contrast, takes place when INPs collide with supercooled droplets, leading to the rapid freezing of the droplets (Murray et al., 2012). Condensation freezing occurs when water vapor condenses onto INP surfaces at subzero temperatures while simultaneously freezing to form ice (Burrows et al., 2022). However, this mechanism remains under debate, as it is not yet clear from a microphysical perspective whether condensation freezing is distinct from immersion freezing or deposition nucleation (Kanji et al., 2017). Therefore, it is not regarded as a separate mechanism in this study.

In the default Morrison cloud microphysics scheme (see Text S1 for details), heterogeneous nucleation parameterization schemes (Bigg, 1953; Cooper, 1986; Meyers et al., 1992) rely solely on temperature or ice supersaturation. However, the combined application of these schemes is still unable to reproduce the observed ice nucleation concentrations (DeMott et al., 2010). In this study, we revised the default Morrison microphysics scheme by incorporating aerosol-aware parameterizations for both mixed-phase clouds (Sect. 2.3.1) and ice clouds (Sect. 2.3.2), which successfully reproduce the observed INP−temperature relationships in natural environments.

2.2.1 Mixed-phase clouds parameterizations

In this study, we improved the representation of ice nucleation in mixed-phase clouds by replacing the Bigg (1953) parameterizations for immersion freezing with those of DeMott et al. (2015), Reicher et al. (2019), and Chen et al. (2021). Deposition nucleation and contact freezing are not included for mixed-phase clouds, as their contribution is generally negligible compared to immersion freezing (Hoose et al., 2008).

DeMott et al. (2015) derived a parameterization scheme for dust INP number concentration as a function of temperature and dust number concentration with diameters larger than 0.5 μm (Eq. (1); hereafter DeMott2015), based on laboratory experiments and field observation datasets of Saharan and Asian desert dust. This

https://doi.org/10.5194/egusphere-2025-5277
Preprint. Discussion started: 18 November 2025

parameterization scheme has since been widely adopted for representing dust INPs in both global and regional models (Shi and Liu, 2019; Kawai et al., 2021; Zeng et al., 2023).

$$n_{\mathrm{INP}}(T) = (\mathrm{cf})(n_{\mathrm{a}} > 0.5\ \mu\mathrm{m})^{(\alpha(273.16-T)+\beta)}\exp(\gamma(273.16-T)+\delta) \quad (1)$$

where $n_{\mathrm{INP}}(T)$ denotes the number concentration of INPs (in std L^{-1}) at temperature T (in K), $n_{\mathrm{a}} > 0.5$ μm represents the number concentration of dust with diameters larger than 0.5 μm (in std cm^{-3}), and the constant coefficients, α, β, γ, and δ, are 0, 1.25, 0.46, and −11.6, respectively. The calibration factor, cf, was set to 3, following DeMott et al. (2015).

Reicher et al. (2019) developed a dust INP parameterization scheme (Eq. (2) and (3); hereafter Reicher2019) for two particle size intervals (0.3 μm < D_{p} < 1 μm and D_p > 1 μm; D_{p} denotes the diameter of dust) based on six dust events in the eastern Mediterranean during 2016–2017, as well as on measurements reported by Price et al. (2018) and Boose et al. (2016).

$$n_{\mathrm{INP}}(T) = n_{\mathrm{s}}(T) \cdot A \quad (2)$$

$$n_{\mathrm{s}}(T) = \exp[y_0 + a/(b + \exp[(T-248)/c])][\mathrm{m}^{-2}] \quad (3)$$

where A is the dust surface area per unit volume of air, $n_{\mathrm{s}}(T)$ is the density of surface active sites of INP (in m^{-2}) at temperature T (in K), and the parameters y_0, a, b, and c are determined by the dust diameter, as listed in Table S1.

Chen et al. (2021), using observational data from East Asian dust events in March and May 2018 and April and May 2019 together with the observational data of Reicher et al. (2019), established parameterizations for five particle size intervals (0.18 μm < D_{p} < 1 μm, 1 μm < D_{p} < 1.8 μm, 1.8 μm < D_{p} < 3.2 μm, 3.2 μm < D_{p} <5.6 μm, 5.6 μm < D_{p} < 10 μm). They reported that the ice-forming efficiency of dust increased with particle size and then leveled off, as decreasing dust number concentration with increasing size limited further enhancement. The parameterization of Chen et al. (2021, hereafter Chen2021) retains the fundamental framework of Reicher2019, but with a modified $n_{\mathrm{s}}(T)$ (Eq. (4)).

$$n_{\mathrm{s}}(T) = \exp(a \cdot T + b)[\mathrm{m}^{-2}] \quad (4)$$

where the values of the parameters a and b depend on the dust diameter, as listed in Table S2.

2.2.2 Ice clouds parameterizations

In the default Morrison microphysics scheme, all aerosol-carrying cloud droplets and raindrops are assumed to homogeneously freeze into ice crystals at temperatures below −40°C. However, under such conditions, heterogeneous nucleation is generally more likely to occur than homogeneous nucleation (Koop et al., 2000; Kanji et al., 2017). At higher, colder, and drier altitudes, deposition nucleation becomes the dominant heterogeneous nucleation pathway.

Previous studies have demonstrated that the competition between homogeneous and heterogeneous nucleation plays a critical role in ice clouds (Liu and Penner, 2005;

https://doi.org/10.5194/egusphere-2025-5277
Preprint. Discussion started: 18 November 2025

Kuebbeler et al., 2014). In ice clouds, homogeneous nucleation of supercooled droplets can produce numerous small ice crystals, whereas heterogeneous nucleation requires lower relative humidity, may occur before homogeneous nucleation, produces fewer but larger ice crystals, and suppresses homogeneous nucleation.

In this study, we implemented the parameterization of Barahona and Nenes (2009) to simulate the competition between homogeneous and heterogeneous nucleation, enabling the model to explicitly represent interactions between these two nucleation pathways. The ice nucleation spectrum integrated in Barahona and Nenes (2009) includes classical nucleation theory, Meyers et al. (1992), Phillips et al. (2007), and Phillips et al. (2008), which is used in this study. The parameterization of Phillips et al. (2008), based on observations, includes deposition nucleation and immersion freezing and accounts for three aerosol types: dust and metal compounds, inorganic black carbon, and insoluble organic aerosols. In this study, only dust INPs were considered. The dust INP number concentration is calculated according to Eq. (5).

$$n_{\mathrm{INP}}(S_{\mathrm{i}},T) = \int_{\log 0.1}^{\infty} \{1 - \exp[-\mu(S_{\mathrm{i}},T)]\} \times \frac{dn}{d\log D_{\mathrm{p}}}\, d\log D_{\mathrm{p}} \tag{5}$$

where $\mu(S_{\mathrm{i}},T)$ is the average number of activated ice embryos per dust particle at ice supersaturation S_{i} *and* temperature T, n is the number concentration of dust particles, and D_{p} (in μm) is the dust particle diameter. $\mu(S_{\mathrm{i}},T)$ is calculated according to Eq. (6).

$$\mu(S_{\mathrm{i}},T) = H(S_{\mathrm{i}},T)\xi(T)\frac{\alpha \cdot n_{\mathrm{INP},1}}{\Omega_1} \times \frac{d\Omega}{dn} \text{ for } T < 0°\mathrm{C} \text{ and } 0 < S_{\mathrm{i}} \le S_{\mathrm{i}}^{\mathrm{w}} \tag{6}$$

where $S_{\mathrm{i}}^{\mathrm{w}}$ denotes the ice supersaturation at water saturation. $H(S_{\mathrm{i}},T)$ is an empirically determined fraction ($0 \le H \le 1$) representing the scarcity of heterogeneous nucleation of ice seen in substantially subsaturated conditions. At water saturation, $H = 1$. When $T < 0°\mathrm{C}$ and $0 < S_{\mathrm{i}} \le S_{\mathrm{i}}^{\mathrm{w}}$, $H(S_{\mathrm{i}},T)$ is defined by Eq. (7). The factor $\xi(T)$ accounts for the observation that droplets containing INPs are typically seen not to freeze at temperatures warmer than about −2°C. At temperatures colder than −5°C and warmer than −2°C, $\xi(T)$ is assigned values of unity and zero, respectively, with a cubic interpolation in between. α is the fractional contribution from dust to the INP concentration inferred from the continuous flow diffusion chamber (CFDC) measurements, and is set to 2/3 for dust. The term Ω is the total surface area concentration of all dust particles with dry diameters larger than 0.1 μm, and Ω_1 represents the component of Ω contributed by aerosols with diameters between 0.1 and 1 μm. $n_{\mathrm{INP},1}$ is the component of n_{INP} due to dust with diameters between 0,1 and 1 μm, parameterized by Phillips et al. (2007) (Eq. (9) and Eq. (10)).

$$H(S_{\mathrm{i}},T) = \min\{f_{\mathrm{c}} + (1 - f_{\mathrm{c}})\delta_0^1[S_{\mathrm{w}}(S_{\mathrm{i}},T), S_{\mathrm{w},0}, 1], 1\} \tag{7}$$

where f_{c} denotes the contribution to H from nucleation modes (e.g., deposition nucleation) under subsaturated conditions, as defined by Eq. (8). $\delta_a^b[y, y_1, y_2]$ denotes a cubic interpolation function used to interpolate y within $[y_1, y_2]$ onto the interval $[a, b]$ (see Text S2). S_{w} is the saturation ratio with respect to water, parameterized following Murphy and Koop (2005). $S_{\mathrm{w},0}$ is the threshold of S_{w} when $H = 0$, which is

https://doi.org/10.5194/egusphere-2025-5277
Preprint. Discussion started: 18 November 2025

set to 0.97.

$$f_c = \delta_0^h(T, T_0, T_0 + \Delta T)\delta_0^1(S_i, S_{i,0}, S_{i,0} + \Delta S_i)/\gamma \quad (8)$$

where h is the small fraction to which δ is reduced by warming over ΔT. $h = 0.15$, $T_0 = -40°C$, $\Delta T = 5°C$, $S_{i,0} = 1 + 10^x(-80°C < T < 0°C)$, and $\Delta S_i = 0.1$ for dust. $x = b_0 + b_1 T + b_2 T^2 + b_3 T^3$, where $b_0 = -1.0261$, $b_1 = -3.1656 \times 10^{-3}$, $b_2 = 5.3938 \times 10^{-4}$, and $b_3 = 8.2584 \times 10^{-6}$. γ is a factor that enhances INP concentration due to bulk-liquid modes and is set to 2.

$$n_{INP} = 1000 \exp[12.96 S_i - 0.639] \times \psi \text{ for } -30°C \le T \le -5°C \quad (9)$$

$$n_{INP} = 1000\{\exp[12.96(S_i - 0.1)]\}^{0.3} \text{ for } -80°C \le T \le -30°C \quad (10)$$

where n_{INP} is the number concentration of INPs (in m^{-3}), including contributions from deposition nucleation, immersion freezing, and condensation freezing. S_i denotes the ice supersaturation, and ψ is a normalization factor set to 0.06.

The parameterization of Barahona and Nenes (2009) has been widely applied in global models and has demonstrated good performance (Liu et al., 2012; Shi et al., 2015). Further details of the parameterization scheme can be found in Barahona and Nenes (2009) and Phillips et al. (2008).

2.3 Model configurations

We employed the WRF-Chem model with a horizontal resolution of 27 km, 23 vertical layers, and a top pressure of 50 hPa, with denser layers within the planetary boundary layer (PBL). The simulation domain covers most of East Asia (14°–60° N, 74°–130° E), as shown in Fig. S1. The simulated period for analysis is spring 2018 (March−May), which corresponds to the peak dust season in East Asia.

Meteorological initial and boundary conditions were obtained from FNL reanalysis data with a temporal resolution of 6 h and a spatial resolution of 1° × 1° (https://gdex.ucar.edu/datasets/d083002/, last access: 28 Oct. 2025). Chemical initial and boundary conditions were acquired from the simulation results of the Community Atmosphere Model with Chemistry (CAM-Chem) with a temporal resolution of 6 h and a spatial resolution of 0.94° × 1.25° (https://www.acom.ucar.edu/cam-chem/cam-chem.shtml, last access: 28 Oct. 2025). Each simulation was initialized five days before the analysis period (March−May 2018) to minimize the influence of initial conditions. The meteorological fields were reinitialized daily using FNL reanalysis data, while the chemical fields were carried over from the previous day's simulation. This treatment allows for continuous chemical evolution and more reliable meteorological conditions (Zeng et al., 2020). Anthropogenic emissions over mainland China were taken from the ABaCAS-EI 2017 inventory (Air Benefit and Cost and Attainment Assessment System–Emission Inventory), while emissions outside China were based on the IIASA 2015 inventory (International Institute for Applied Systems Analysis) (Zheng et al., 2019; Gao et al., 2020; Li et al., 2023).

The major physical parameterizations employed in this study include the rapid radiative transfer model for GCMs (RRTMG) shortwave and longwave radiative

https://doi.org/10.5194/egusphere-2025-5277
Preprint. Discussion started: 18 November 2025

transfer schemes (Iacono et al., 2008), the revised MM5 Monin-Obukhov surface layer scheme (Jiménez et al., 2012), the unified Noah land surface scheme (Tewari et al., 2004), Yonsei University (YSU) PBL scheme (Hong et al., 2006), and the Grell-Freitas ensemble cumulus scheme (Grell and Freitas, 2014). For atmospheric chemistry, we employed version 1999 of the Statewide Air Pollution Research Center mechanism (SAPRC-99; Carter, 2000) gas-phase chemistry mechanism and the MOSAIC aerosol chemistry module using a 20-bin size representation.

2.4 Experimental design

Six simulation scenarios, summarized in Table 1, were designed to investigate the impacts of dust INPs on clouds and radiation, with all scenarios sharing identical model configurations except for the treatment of ice nucleation. In this study, heterogeneous nucleation in mixed-phase clouds included immersion freezing, whereas that in ice clouds comprised both deposition nucleation and immersion freezing. The heterogeneous and homogeneous nucleation processes for each scenario were specified as follows:

- **NoINPs**: Heterogeneous nucleation was turned off in both mixed-phase and ice clouds, while homogeneous nucleation of cloud droplets was active.
- **MixINPs**: Heterogeneous nucleation was enabled in mixed-phase clouds by employing the immersion freezing scheme of Chen2021, while heterogeneous nucleation in ice clouds remained off. Homogeneous nucleation was active.
- **IceINPs**: Heterogeneous nucleation was enabled in ice clouds, while heterogeneous nucleation in mixed-phase clouds was off. Homogeneous nucleation was active.
- **MixIceINPs**: Heterogeneous nucleation was enabled in both mixed-phase and ice clouds. The immersion freezing process followed the parameterization of Chen2021. Homogeneous nucleation was active.
- **MixINPs_DeMott2015**: Similar to MixINPs, but immersion freezing in mixed-phase clouds employed the scheme of DeMott2015.
- **MixINPs_Reicher2019**: Similar to MixINPs, but immersion freezing in mixed-phase clouds employed the scheme of Reicher2019.

Only dust was considered as INPs in this study. To separate the effects of aerosol ice nucleation from the thermodynamic impacts of aerosols on cloud microphysics resulting from changes in solar radiation, dust emissions were activated in the NoINPs scenario to maintain consistent thermodynamic conditions with other scenarios, but heterogeneous ice nucleation by dust was not considered. In all scenarios, aerosol–radiation interactions were enabled, so that the direct radiative effects of dust were consistently represented. The differences MixINPs – NoINPs, IceINPs – NoINPs, and MixIceINPs – NoINPs represented the indirect effects of dust INPs in mixed-phase clouds, ice clouds, and both cloud types, respectively. For mixed-phase cloud immersion freezing, the scheme of Chen2021 was applied in MixINPs, as it shows the

https://doi.org/10.5194/egusphere-2025-5277
Preprint. Discussion started: 18 November 2025

best performance in reproducing dust INPs (see Sect. 3.1). To assess sensitivity to different parameterizations, two additional experiments, MixINPs_DeMott2015 and MixINPs_Reicher2019, employed alternative immersion freezing schemes. Comparisons among MixINPs, MixINPs_DeMott2015, and MixINPs_Reicher2019 allowed evaluation of the uncertainties associated with different parameterizations, particularly regarding dust particle size effects.

Table 1. Ice nucleation treatments in six simulation scenarios designed to investigate the effects of dust INPs on clouds and radiation. Heterogeneous nucleation in ice clouds and homogeneous nucleation followed Barahona and Nenes (2009). All other model configurations were identical.

Scenarios	Mixed-phase cloud heterogeneous nucleation	Mixed-phase cloud immersion freezing scheme	Ice cloud heterogeneous nucleation	Homogeneous nucleation
NoINPs	Off	/	Off	On
MixINPs	On	Chen2021	Off	On
IceINPs	Off	/	On	On
MixIceINPs	On	Chen2021	On	On
MixINPs_DeMott2015	On	DeMott2015	Off	On
MixINPs_Reicher2019	On	Reicher2019	Off	On

2.5 Measurements

Surface PM_{10} concentrations were obtained from the National Environmental Monitoring Center of China (https://quotsoft.net/air/, last access: 28 Oct. 2025). For model–observation comparison, simulated PM_{10} values were extracted from the nearest grid cell to each monitoring station. Monthly aerosol optical depth (AOD), IWP, and LWP were derived from the Moderate Resolution Imaging Spectroradiometer (MODIS) onboard the Aqua satellite, using the MYD08_M3 (Collection 6.1) product with a spatial resolution of 1° × 1° (https://ladsweb.modaps.eosdis.nasa.gov/, last access: 28 Oct. 2025). Modeled AOD was compared with MODIS retrievals at the wavelength of 550 nm, obtained using the Combined Dark Target and Deep Blue algorithms.

Dust INPs under mixed-phase cloud conditions were derived from aerosol samples collected at the Peking University Atmospheric Environment Monitoring Station (116.31° E, 39.99° N), a typical urban site influenced by East Asian dust transport, using the Peking University Ice Nucleation Array (PKU-INA) during two representative dust events on 1 and 26 May 2018, covering temperatures from −5°C to −25°C (Chen et al., 2021). PKU-INA is a cold-stage-based instrument designed for immersion freezing measurements. For comparison with observations, modeled INP concentrations were diagnosed offline using parameterization schemes and simulated aerosol properties. Particle number size distributions (PNSDs) from 3 nm to 10 μm were measured with two scanning mobility particle sizers (SMPS) and an aerodynamic particle sizer (APS). Further details of the measurement setup can be found in Chen et al. (2021).

Dust INPs under ice cloud conditions were derived from ambient aerosol samples collected on 22 May 2014 at the Kuqa Meteorological Bureau (83.04° E, 41.43° N) in the Aksu region of Xinjiang, China, with INP concentrations measured using a Static

https://doi.org/10.5194/egusphere-2025-5277
Preprint. Discussion started: 18 November 2025

Vacuum Diffusion Cloud Chamber (Jiang et al., 2016). The deposition mode measurements were performed at following temperatures (ice supersaturations): −14°C (5%, 8%, 12%, 15%), −16°C (5%, 8%, 12%, 17%), −18°C (5%, 8%, 12%, 16%, 20%), and −20°C (5%, 8%, 12%, 16%, 20%, 22%). Although the Phillips et al. (2008) parameterization accounts for both immersion freezing and deposition nucleation, the observations represent deposition nucleation only. The contribution from immersion freezing is likely negligible, as the site is located near the Taklamakan Desert, where anthropogenic pollution is minimal and deposition nucleation dominates dust ice formation. PNSDs from 0.1 μm to 10 μm were measured using a Passive Cavity Aerosol Spectrometer Probe (PCASP) and an APS. Additional information is provided in Jiang et al. (2016).

3 Results and discussion

3.1 Model evaluation

To evaluate the accuracy and reliability of the model, the simulated results were compared with multiple observational datasets. The evaluation focused on surface PM_{10} mass concentration, AOD, IWP, LWP, and dust INP number concentration in both mixed-phase clouds and ice clouds.

The simulated monthly mean surface PM_{10} mass concentrations for March–May 2018 are evaluated against observations from 1,035 sites within the domain shown in Fig. 1a. In March 2018 (Fig. 1a), the observed site-averaged monthly mean is 95.13 μg m^{-3}, whereas the simulated mean is 68.6 μg m^{-3}, corresponding to an overall underestimation of 28%. The bias is more pronounced near the Taklamakan Desert than over the Gobi Desert or in eastern China, likely due to an inaccurate representation of soil particle size distribution (Zeng et al., 2020). In April 2018 (Fig. 1b), the model slightly overestimates PM_{10} concentrations by 2% on average, with underestimation near the Taklamakan Desert and eastern China and overestimation over the Gobi Desert. In May 2018 (Fig. 1c), the simulated monthly mean concentrations are generally consistent with the observations, capturing the observed spatial distribution with a normalized mean bias (NMB) of −8% and a spatial correlation coefficient (R) of 0.64. Overall, the model reasonably reproduces the spatial distribution of PM_{10} and performs comparably to previous studies (Su and Fung, 2018a; Zeng et al., 2020).

https://doi.org/10.5194/egusphere-2025-5277
Preprint. Discussion started: 18 November 2025

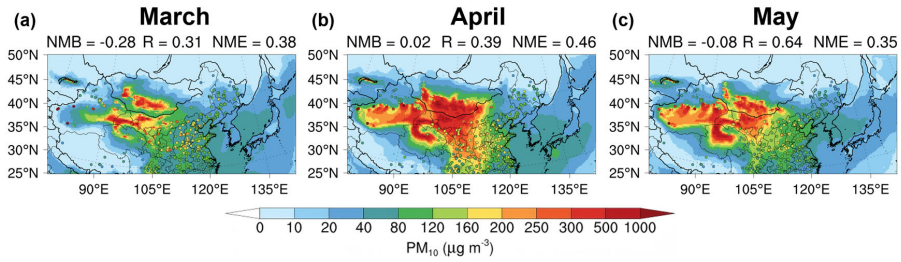

Figure 1. Comparison between simulated and observed surface monthly mean PM_{10} mass concentrations in **(a)** March, **(b)** April, and **(c)** May 2018. Circles denote monthly mean observations from 1035 sites, and color shading indicates the corresponding simulated monthly means. The statistics shown above each panel include the normalized mean bias (NMB), normalized mean error (NME), and correlation coefficient (R). The simulated results are from the MixIceINPs scenario and represent averages of hourly values.

The modeled monthly mean AOD for March–May 2018 is evaluated against MODIS observations. In March 2018 (Fig. S2a and S2d), AOD is underestimated over the Taklamakan Desert, consistent with the PM_{10} underestimation since dust dominates the aerosol burden in this region. The model reproduces the elevated AOD in eastern China, mainly driven by anthropogenic emissions, with minor spatial discrepancies that are acceptable given that anthropogenic pollution is not the focus of this study. In April (Fig. S2b and S2e), AOD is slightly underestimated over the Taklamakan Desert and overestimated over the Gobi Desert, consistent with the PM_{10} distribution. In May (Fig. S2c and S2f), AOD remains overestimated over the Gobi Desert. Overall, the model reasonably captures the spatial distribution of AOD.

The simulated monthly mean IWP and LWP for March–May 2018 are evaluated against MODIS observations (Fig. S3). The simulated IWP is in satisfactory agreement with the observations and reproduces their spatial distribution. The simulated LWP also shows good agreement with observations over the Yangtze River Delta in China and Japan, although noticeable discrepancies remained in northern China. These differences may have resulted from limitations in the cloud parameterization schemes in the model or from uncertainties in the retrievals from the MODIS dataset. Overall, the model reproduces the spatial distribution of both IWP and LWP reasonably well, providing a useful basis for assessing the impacts of dust INPs on clouds and radiation.

The simulated dust INP concentrations under mixed-phase cloud conditions are evaluated against observations at Peking University on 1 and 26 May 2018 (Chen et al., 2021). On both days, simulations with Chen2021 reproduces the observed INP concentrations within one order of magnitude across most temperatures, outperforming both DeMott2015 and Reicher2019 (Fig. 2a). On 1 May 2018, Chen2021 underestimates INPs but remaines within one order of magnitude, while DeMott2015 agrees well between –6°C and –12°C and near –18°C but overestimates in the –12°C to –18°C range. Reicher2019 showed larger deviations than Chen2021 at all

https://doi.org/10.5194/egusphere-2025-5277
Preprint. Discussion started: 18 November 2025

temperatures. On 26 May 2018, Chen2021 overestimates INPs between –6°C and –9°C and underestimates between –9°C and –20°C, yet errors still remain within one order of magnitude. In contrast, DeMott2015 overestimates INPs at all temperatures, whereas Reicher2019 underestimates below –9°C and overestimates above –9°C, again with larger errors than Chen2021.

Biases in simulated dust INP concentrations are closely linked to errors in simulated dust number or surface area concentrations. In the absence of dust number observations, simulated PNSDs are used for evaluation, which is reasonable since dust dominated the aerosol composition during both events. On 1 May 2018 (Fig. 2c), the model underestimates aerosol number concentrations in the 1–10 μm range by up to one order of magnitude. Correcting this underestimate would improve the agreement of Chen2021 with the observations but exacerbate the overestimation by DeMott2015. On 26 May (Fig. 2c), the model overestimates aerosol number concentrations in the 0.1–2 μm range and slightly underestimates in the 2–10 μm range, likely contributing to the modest overestimation of INPs in Fig. 2a. However, since the observations represent total INPs from all aerosol types while the simulations consider dust only, some compensating biases may exist.

Overall, DeMott2015 predicts INP concentrations about five and ten times higher than Chen2021 on 1 and 26 May, respectively, at a representative urban site influenced by East Asian dust transport. This discrepancy may be associated with the use of uniform parameters for all dust particles larger than 0.5 μm in DeMott2015, which could overrepresent the ice-forming efficiency of smaller particles. In DeMott et al. (2015), the predicted INP concentrations were in excellent agreement with those from the aerosol-surface-area-based parameterization of (Niemand et al., 2012), whereas Chen et al. (2021) found that their parameterization for the 5.6–10 μm size interval is consistent with the Niemand et al. (2012) scheme. These findings suggest that the DeMott2015 parameterization is more suitable for representing larger dust particles (> 5.6 μm), while Chen et al. (2021) further indicate that the ice-forming efficiency of dust increases with particle size. However, at this observation site, smaller dust particles (0.18–3.2 μm) contribute over 95% of the total dust surface area (Fig. S4), implying that large-particle-oriented schemes may overestimate INP concentrations under such conditions. Because smaller dust particles can be transported to higher altitudes and over long distances, DeMott2015 is likely to predict higher INP concentrations aloft and downwind of dust sources. By incorporating size-resolved effects, Chen2021 offers an alternative representation that may better capture the spatial variability of dust INPs.

The simulated dust INP concentrations under ice cloud conditions are evaluated against observations at a station located near the Taklimakan Desert, China (Jiang et al. 2016). As the observational data were obtained on 22 May 2014, the period from 14 to 25 May 2014 is simulated using the same model configuration as in the IceINPs scenario. As shown in Fig. 2b, the error between the simulation and observation decreased with decreasing temperature, but the model increasingly overestimated INPs with higher ice supersaturation at a given temperature. At −14°C, simulated INP

https://doi.org/10.5194/egusphere-2025-5277
Preprint. Discussion started: 18 November 2025

concentrations deviated from observations by about one order of magnitude, whereas at −20°C the maximum deviation was a factor of 5. These errors likely arise from biases in simulated aerosol number concentrations. To further investigate, the simulated PNSDs on 22 May 2014 were compared with measurements (Fig. 2c). The model generally overestimated aerosol number concentrations in the 0.1–10 μm range, with the smallest bias (near agreement) at 1 μm. The overestimation was within one order of magnitude for particles between 1 and 10 μm, but reached up to two orders of magnitude in the 0.1–1 μm range. The overestimation of aerosol number concentrations in the 0.1–10 μm range explains the overestimation of dust INP number concentrations.

In summary, the performance of the model in simulating dust, dust INP, and cloud water over East Asia is fairly good, and the discrepancies between the simulations and observations are reasonable and acceptable.

https://doi.org/10.5194/egusphere-2025-5277
Preprint. Discussion started: 18 November 2025

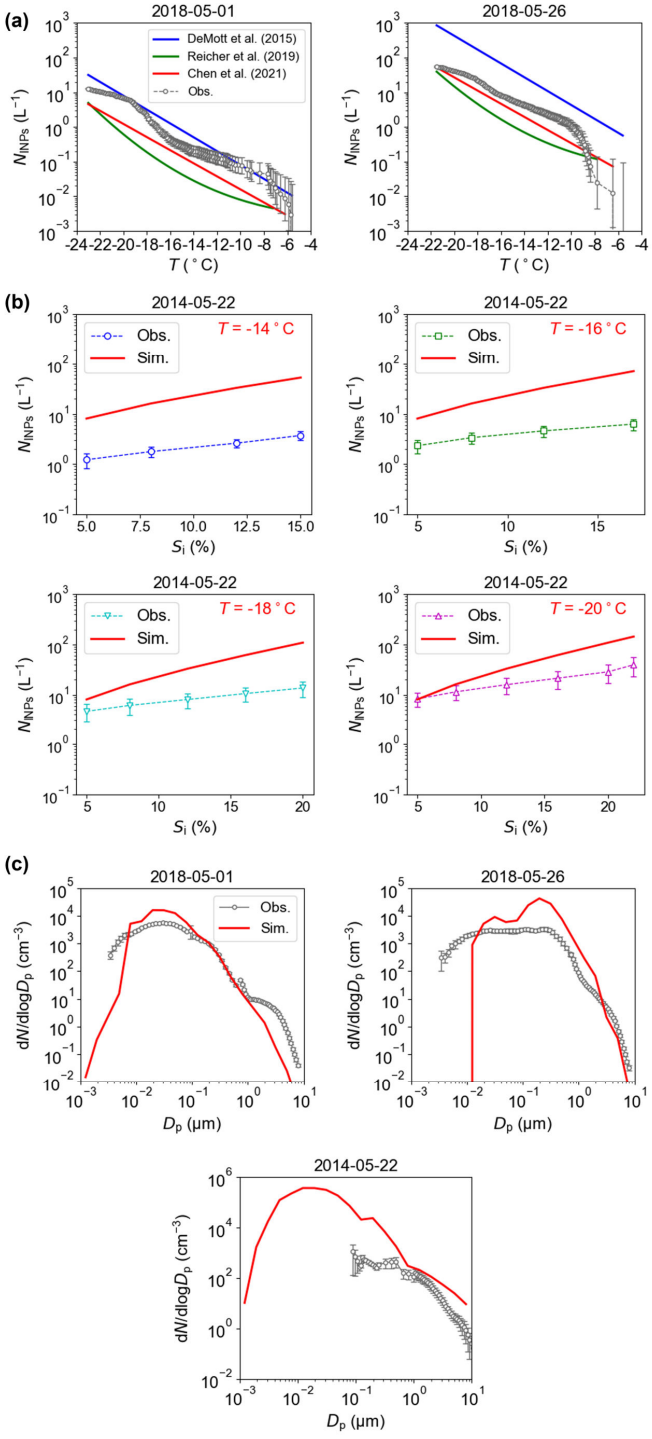

https://doi.org/10.5194/egusphere-2025-5277
Preprint. Discussion started: 18 November 2025

Figure 2. Comparison of simulated and observed dust INP number concentrations and particle number size distributions (PNSDs). **(a)** Simulated dust INP number concentrations in mixed-phase clouds compared with observations on 1 and 26 May 2018 at the Peking University Atmosphere Environment Monitoring Station (116.31° E, 39.99° N). N_{INPs} denotes the number concentration of dust INPs, and T denotes the temperature. **(b)** Simulated dust INP number concentrations in ice clouds compared with observations at −14°C, −16°C, −18°C, and −20°C on 22 May 2014 at the Kuqa Meteorological Bureau (83.04° E, 41.43° N) in the Aksu region of Xinjiang, China. S_i denotes ice supersaturation, Obs. denotes observations, and Sim. denotes simulations. **(c)** Simulated PNSDs compared with observations from the same stations and dates as in panels (a) and (b). N denotes the aerosol number concentration, and D_p denotes the aerosol diameter. Error bars indicate the 95% confidence intervals for the observations. The simulated results are from the MixIceINPs scenario and represent averages of hourly values.

3.2 Impacts of dust INPs on clouds and radiation

3.2.1 Spatial distribution of dust INPs

Figure 3 shows the meridionally averaged vertical cross-sections of dust INPs and ice crystals formed by homogeneous nucleation for each scenario. Unless otherwise noted, the simulations are averaged over March–May 2018. For the NoINPs scenario, ice crystals formed through homogeneous nucleation are mainly found at temperatures below −40°C. The occurrence of ice crystals formed through homogeneous nucleation at temperatures greater than −37°C is noted, which is due to temporal averaging and meridional averaging.

For the MixINPs scenario, the distribution of ice crystals formed by homogeneous nucleation closely resembles that in NoINPs, whereas dust INPs in mixed-phase clouds are mainly distributed below the −40°C isotherm. The mean concentration of INPs in mixed-phase clouds (1.8×10^{-3} L^{-1}) is about one order of magnitude lower than that of ice crystals from homogeneous nucleation (1.7×10^{-2} L^{-1}).

For the IceINPs scenario, INPs in ice clouds are also mainly distributed at temperatures below −40°C. The mean concentration of ice crystals formed from homogeneous nucleation (9.1×10^{-4} L^{-1}) in IceINPs is only 5.4% of that in NoINPs, indicating strong suppression of homogeneous nucleation by heterogeneous nucleation. By contrast, the mean concentration of INPs in ice clouds (3.7×10^{-1} L^{-1}) is about 22 times higher than that of ice crystals formed through homogeneous nucleation in NoINPs, which may be due to the relatively low ice supersaturation limiting the occurrence of homogeneous nucleation. Homogeneous nucleation mainly occurs at ice saturation greater than 1.3, but grid cells with ice saturation greater than 1.3 account for less than 0.7% of the grids at temperatures below −37°C (Fig. S5). This higher concentration of INPs relative to homogeneous ice crystals is further supported by high dust concentrations at temperatures below −40°C (Fig. S6a) and by the fact that heterogeneous nucleation can occur at warmer temperatures and lower ice

https://doi.org/10.5194/egusphere-2025-5277
Preprint. Discussion started: 18 November 2025

supersaturation. Overall, INPs in ice clouds are about 206 times more abundant than INPs in mixed-phase clouds in MixINPs, reflecting that ice-phase conditions are more favorable for heterogeneous nucleation.

For the MixIceINPs scenario, the concentrations of ice crystal number formed by homogeneous nucleation and dust INPs in ice clouds are similar to those in IceINPs. However, the mean concentration of dust INPs in mixed-phase clouds (1.9×10^{-4} L^{-1}) is about one order of magnitude lower than in MixINPs. This reduction is likely related to latent heat release during heterogeneous nucleation in ice clouds, which increases temperatures in the mixed-phase layer (Fig. S8b).

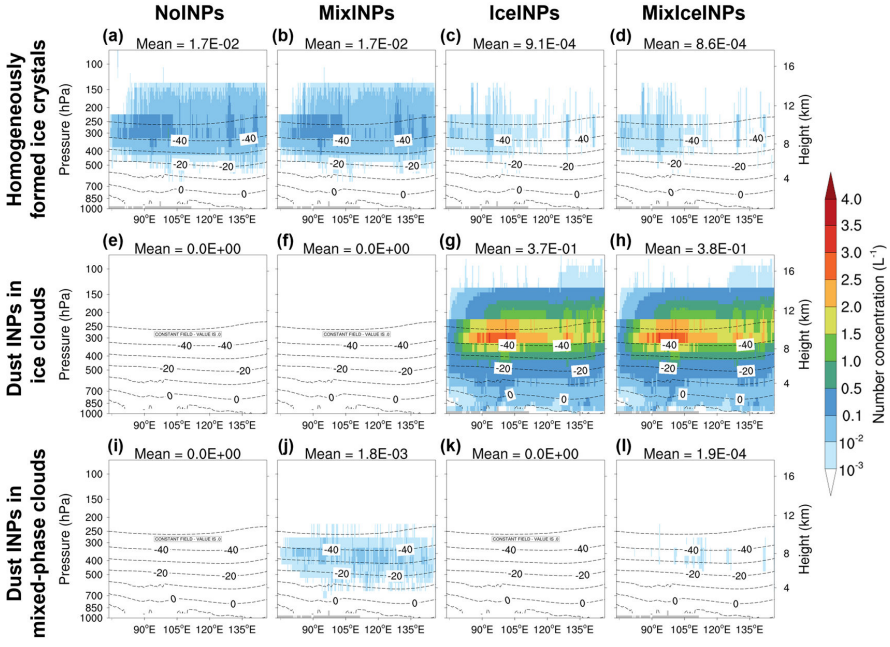

Figure 3. Simulated meridional mean vertical cross-sections of **(a–d)** homogeneously formed ice crystals, **(e–h)** dust INPs in ice clouds, and **(i–l)** dust INPs in mixed-phase clouds, for the NoINPs (first column), MixINPs (second column), IceINPs (third column), and MixIceINPs (fourth column) scenarios. Dashed lines indicate isotherms, and grey shading denotes missing values due to terrain. The mean value over the plotted region is shown above each panel. The simulated results are averages of hourly values from March to May 2018.

The horizontal distributions of dust INP number concentrations under different scenarios are presented (Fig. 4). Dust INPs in ice clouds are analyzed at 250 hPa, representing a typical ice cloud altitude, while dust INPs in mixed-phase clouds are analyzed at 450 hPa, representing a typical mixed-phase cloud altitude (Hoinka, 1998). For the MixINPs scenario, dust INPs in mixed-phase clouds are mainly concentrated over dust source regions, with substantially lower values in downwind areas, likely due to the removal of coarse particles during long-range transport (Fig. S7). Notably, the

https://doi.org/10.5194/egusphere-2025-5277
Preprint. Discussion started: 18 November 2025

Qinghai–Tibetan Plateau appears as a hotspot of dust INPs in mixed-phase clouds, suggesting their potential influence on cloud and radiation processes over this region. For the IceINPs scenario, dust INPs in ice clouds are more evenly distributed between source and downwind regions, as they are primarily contributed by fine dust particles that can be transported over longer distances. For the MixIceINPs scenario, a suppression effect of dust INPs in mixed-phase clouds by those in ice clouds is also evident.

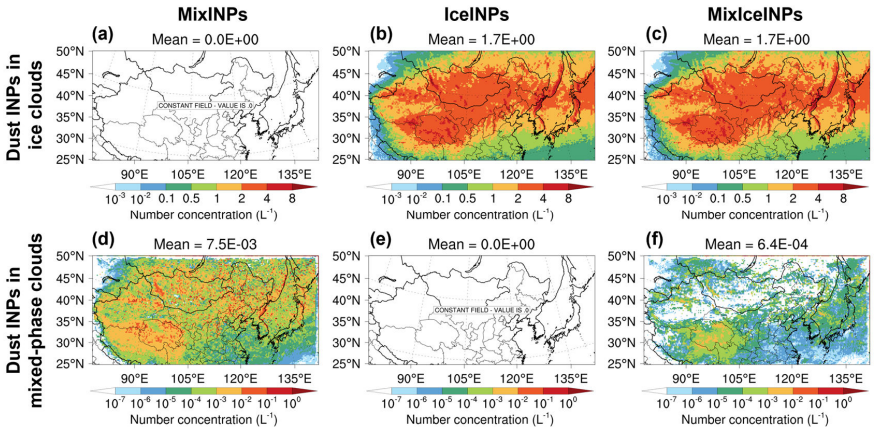

Figure 4. Simulated spatial distributions of **(a–c)** dust INP number concentrations in ice clouds at 250 hPa and **(d–f)** dust INP number concentrations in mixed-phase clouds at 450 hPa, for the MixINPs (left column), IceINPs (middle column), and MixIceINPs (right column) scenarios. The mean value over the plotted region is shown above each panel. The simulated results are averages of hourly values from March to May 2018.

3.2.2 Impacts of dust INPs on clouds

The meridionally averaged vertical cross-section of ice-phase and liquid-phase variables is shown in Fig. 5. For the NoINPs scenario, ice crystals are mainly found at temperatures below −40°C, consistent with ice crystals formed by homogeneous nucleation. The effective radius of ice crystals tends to be larger between −40°C and −20°C, with smaller radii at the upper and lower boundaries of this range. This pattern reflects gravitational sedimentation of larger ice crystals, during which rising temperature enhances the saturation vapor pressure. When the ambient vapor pressure falls below the saturation level, sublimation occurs and reduces crystal size. The distribution of ice water content shows a similar pattern, though with maximum values between −30°C and −10°C. The number concentration of cloud droplets decreases steadily with altitude. The effective radius of cloud droplets remains nearly uniform vertically, but increases gradually eastward. This east–west contrast likely arises from differences in water vapor supply, as the domain is bounded by the Pacific Ocean to the east and the Taklamakan Desert to the west. The vertical distribution of liquid water

https://doi.org/10.5194/egusphere-2025-5277
Preprint. Discussion started: 18 November 2025

content largely mirrors that of droplet number concentration.

For the MixINPs scenario, dust-induced ice nucleation in mixed-phase clouds enhances the number concentration of ice crystals, the effective radius of ice crystals, and ice water content, while reducing the number concentration of cloud droplets and liquid water content, but increasing droplet mean radius. These changes are caused by the acceleration of the WBF process by dust particles (Liu et al., 2011). Dust INPs initiate additional ice crystals, increasing crystal number concentration, while the WBF process transfers mass from liquid to ice, promoting crystal growth. The combined increase in number concentration and radius leads to higher ice water content. Small droplets, with higher saturation vapor pressures, evaporate preferentially during WBF, leaving fewer but larger droplets, thus lowering droplet concentration, enlarging their mean radius, and reducing liquid water content.

For the IceINPs scenario, ice crystal number concentration in ice clouds ($< -37°C$) increases sharply because dust INP concentrations are about 22 times larger than the concentration of ice crystals formed via homogeneous nucleation in the NoINPs scenario. Under a fixed water content, this increase in number concentration reduces crystal radius, an effect analogous to the Twomey effect (Twomey, 1974). This contrasts with the global-scale "anti-Twomey effect" reported in Liu et al. (2012), Kuebbeler et al. (2014), and Beer et al. (2024), as here the dust INP concentrations in ice clouds greatly exceed those of homogeneously nucleated crystals. Although the effective radius decreases, the increase in number concentration dominates, leading to enhanced ice water content in ice clouds. Moreover, precipitation of ice crystals from ice clouds into mixed-phase clouds further increases ice crystal number concentration there, reinforcing the WBF process. This produces larger ice crystals, higher ice water content, fewer cloud droplets, larger droplet mean radius, and reduced liquid water content in mixed-phase clouds. The magnitude of these changes in the IceINPs scenario exceeds those in MixINPs, because the flux of ice crystals sedimenting from ice clouds into mixed-phase clouds is greater than the number of crystals nucleated in situ by dust INPs. As a result, the influence of dust INPs in ice clouds dominates over those in mixed-phase clouds, and the outcomes of MixIceINPs and IceINPs are nearly identical.

https://doi.org/10.5194/egusphere-2025-5277
Preprint. Discussion started: 18 November 2025

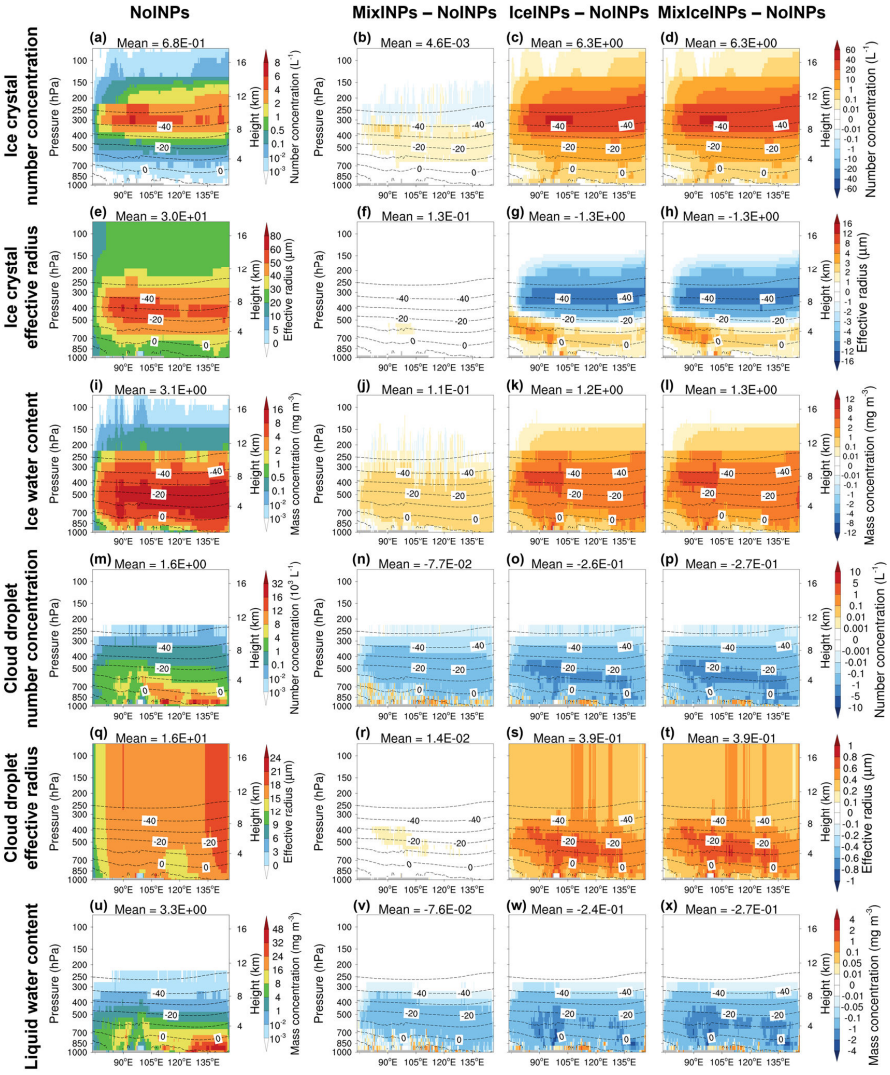

Figure 5. Simulated meridional mean vertical cross-sections of **(a–d)** ice crystal number concentration, **(e–h)** ice crystal effective radius, **(i–l)** ice water content, **(m–p)** cloud droplet number concentration, **(q–t)** cloud droplet effective radius, and **(u–x)** liquid water content, for the NoINPs (first column), MixINPs – NoINPs (second column), IceINPs – NoINPs (third column), and MixIceINPs – NoINPs (fourth column) scenarios. Dashed lines indicate isotherms, and grey shading denotes missing values due to terrain. The mean value over the plotted region is shown above each panel. The simulated results are averages of hourly values from March to May 2018.

The horizontal distributions of ice-phase and liquid-phase variables are presented (Fig. 6). For this analysis, the ice crystal number concentration, cloud droplet number concentration, ice water content, and liquid water content were vertically integrated to

https://doi.org/10.5194/egusphere-2025-5277
Preprint. Discussion started: 18 November 2025

obtain column concentrations, while the effective radii of ice crystals and cloud droplets were vertically averaged.

For the NoINPs scenario, higher values of ice crystal column number concentration occur along Qinghai–Gansu–Inner Mongolia–Northeast–Japan. Larger ice crystal effective radii are found over the Qinghai–Tibetan Plateau and Northeast Asia, where lower temperatures favor ice crystal growth. High IWP values are located over the western Pacific, the Qinghai–Tibetan Plateau, and the middle–lower Yangtze River plain, consistent with higher water content (see the spatial distribution of temperature and total water column mass concentration in Fig. S9). Elevated cloud droplet number concentrations in the Yangtze River plain are associated with higher moisture and temperatures compared to the Plateau and northern regions. The distribution of cloud droplet effective radius resembles that of ice crystals, while LWP broadly follows the distribution of cloud droplet column number concentration.

For the MixINPs scenario, ice crystal column number concentration increases slightly in most regions. The effective radius of ice crystals is larger over the Qinghai–Tibetan Plateau and dust source regions, driven by the enhanced WBF process induced by dust INPs in mixed-phase clouds. On average, IWP increases by 2.3%, cloud droplet column number concentration decreases by 7.8%, cloud droplet mean effective radius increases by 0.2%, and LWP decreases by 3.3%.

For the IceINPs scenario, dust INPs in ice clouds lead to an average increase of 86.7% in ice crystal column number concentration and 29.1% in IWP across the domain. The increase in ice crystal effective radius over the Tibetan Plateau and northern regions is likely associated with lower temperatures in these regions, where ice crystals sedimenting from ice clouds into mixed-phase clouds grow larger via the WBF process, with the increase in ice crystal effective radius in mixed-phase clouds exceeding the decrease in ice clouds. Ice crystals precipitating from ice clouds into mixed-phase clouds accelerate the WBF process, resulting in an average 23.3% decrease in cloud droplet column number concentration, a 2.5% increase in cloud droplet mean effective radius, and a 9.5% decrease in LWP. These changes are more pronounced over the Qinghai–Tibetan Plateau and northern regions than elsewhere. Results for the MixIceINPs scenario are generally consistent with those of the IceINPs scenario.

https://doi.org/10.5194/egusphere-2025-5277
Preprint. Discussion started: 18 November 2025

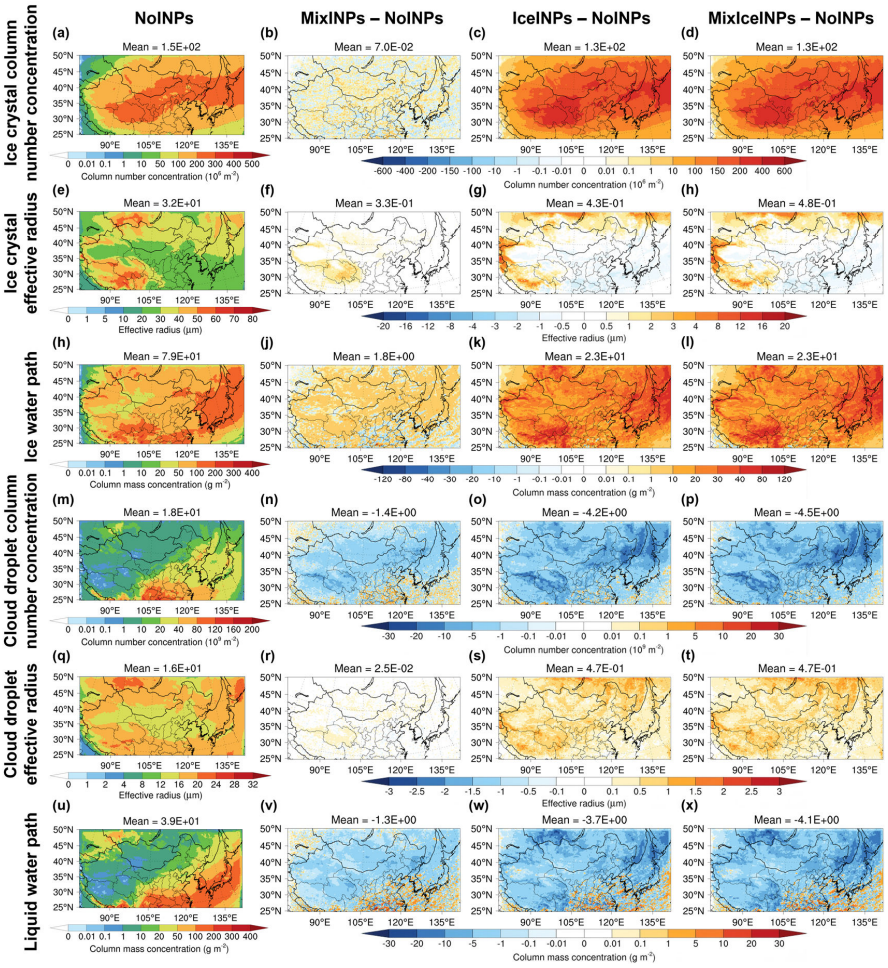

Figure 6. Simulated spatial distributions of **(a–d)** ice crystal column number concentrations (vertically integrated), **(e–h)** ice crystal effective radius (vertically averaged), **(i–l)** ice water path, **(m–p)** cloud droplet column number concentrations (vertically integrated), **(q-t)** cloud droplet effective radius (vertically averaged), and **(u–x)** liquid water path, for the NoINPs (first column), MixINPs – NoINPs (second column), IceINPs – NoINPs (third column), and MixIceINPs – NoINPs (fourth column) scenarios. The mean value over the plotted region is shown above each panel. The simulated results are averages of hourly values from March to May 2018.

To enhance the robustness of the simulation results, monthly averages were calculated and analyzed. Figure S10 presents the horizontal monthly means of ice-phase and liquid-phase variables. Overall, the direction and magnitude of changes for each variable in individual months are consistent with the results from multi-month averages, except for the effective radius of ice crystals in May 2018. In this case, the difference between the IceINPs and NoINPs scenarios is a very small negative value, arising from

https://doi.org/10.5194/egusphere-2025-5277
Preprint. Discussion started: 18 November 2025

compensating regional signals where the effective radius of ice crystals increases in some areas but decreases in others.

For all variables, the perturbations induced by dust INPs in ice clouds are larger than those induced by dust INPs in mixed-phase clouds. In mixed-phase clouds, the increase in ice crystal column number concentration is much smaller than the corresponding decrease in cloud droplet column number concentration; the enhancement in the effective radius of ice crystals is about one order of magnitude larger than the enhancement in cloud droplet effective radius; and the increase in IWP slightly exceeds the decrease in LWP. In contrast, for dust INPs in ice clouds, the increase in ice crystal column number concentration is greater than the decrease in cloud droplet column number concentration, the increase in the effective radius of ice crystals is slightly larger than the increase in cloud droplet effective radius, and the increase in IWP clearly exceeds the decrease in LWP. These findings are consistent with the results reported by Su and Fung (2018b).

3.2.3 Impacts of dust INPs on radiation

The radiative effects of dust INPs in mixed-phase and ice clouds at the top of the atmosphere are shown in Fig. 7. For the MixINPs scenario, shortwave radiation over the simulated region increases by an average of 0.35 W m^{-2}, longwave radiation decreases by an average of 0.15 W m^{-2}, and net radiation increases by an average of 0.20 W m^{-2}. The presence of dust INPs in mixed-phase clouds accelerates the WBF process, leading to more numerous and larger ice crystals, fewer cloud droplets, and a larger cloud droplet mean radius. These changes reduce cloud albedo, allowing more shortwave radiation to enter and more longwave radiation to escape. Because the increase in shortwave radiation exceeds the decrease in longwave radiation, the net effect is an increase in net radiation. The radiative effect of dust INPs in mixed-phase clouds found here contrasts with the results of Shi and Liu (2019) and Kawai et al. (2021), where increases in low-cloud fraction and decreases in droplet radius offset the shortwave response to reduced LWP. In this study, no such changes in low-cloud fraction or droplet radius are evident.

For the IceINPs scenario, shortwave radiation decreases by an average of 5.73 W m^{-2}, longwave radiation increases by an average of 9.29 W m^{-2}, and net radiation increases by an average of 3.56 W m^{-2}. Dust INPs in ice clouds enhance heterogeneous nucleation, producing more ice crystals with a smaller radius and higher ice water content. These processes intensify ice cloud formation, resulting in greater reflection of shortwave radiation to space and stronger trapping of longwave radiation within the atmosphere. Because the longwave effect dominates, the net radiation increases, strengthening the warming effect of ice clouds. This behavior reflects the Twomey effect and leads to a radiative response opposite to the globally averaged results reported by Liu et al. (2012), Kuebbeler et al. (2014), and Beer et al. (2024).

Monthly calculations (Fig. S11) show radiative effects with consistent sign and

https://doi.org/10.5194/egusphere-2025-5277
Preprint. Discussion started: 18 November 2025

magnitude compared to the three-month averages, confirming the robustness of our simulation results.

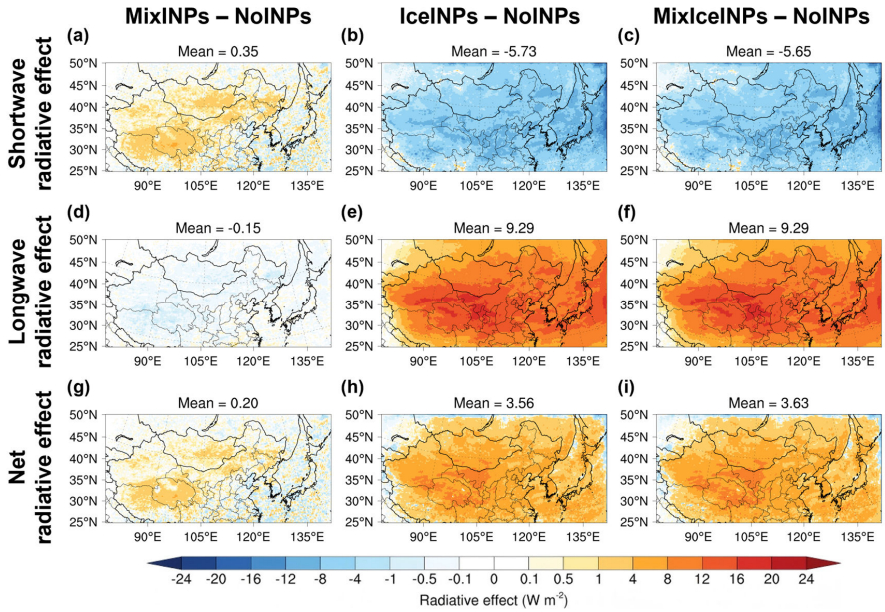

Figure 7. Simulated spatial distributions of **(a–c)** shortwave radiative effect, **(d–f)** longwave radiative effect, and **(g–i)** net radiative effect of dust INPs at the top of the atmosphere (left column: MixINPs – NoINPs; middle column: IceINPs – NoINPs; right column: MixIceINPs − NoINPs). The mean value over the plotted region is shown above each panel. The simulated results are averages of hourly values from March to May 2018.

3.2.4 Comparison of INP parameterization schemes

The meridional averaged vertical cross-section differences between simulations employing the DeMott2015 and Reicher2019 schemes for mixed-phase clouds and those employing the Chen2021 scheme are presented (Fig. 8). Simulations with DeMott2015 produced higher dust INP concentrations than Chen2021, particularly between the –20°C and –40°C isotherms, with an average increase by a factor of 2.1. Consistently, DeMott2015 yielded higher ice water content (mean: 5.8×10^{-2} mg m^{-3}) and lower liquid water content (mean: 4.5×10^{-2} mg m^{-3}) compared to Chen2021, suggesting enhanced activity of the WBF process and stronger liquid-to-ice conversion due to elevated INP concentrations. Notably, the mean liquid water content difference between DeMott2015 and Chen2021 (-4.5×10^{-2} mg m^{-3}) is comparable to that between Chen2021 and simulations without dust INPs (MixINPs – NoINPs; Fig. 5v; -7.6×10^{-2} mg m^{-3}), underscoring that the choice of parameterization can induce differences as large as the inclusion or exclusion of dust INPs.

In contrast, Reicher2019 produced lower dust INP concentrations than Chen2021

https://doi.org/10.5194/egusphere-2025-5277
Preprint. Discussion started: 18 November 2025

between the 0°C and –20°C isotherms, but higher concentrations at temperatures below –20°C. The underestimation in the warmer temperature range is consistent with evaluation against observations (Fig. 2a). Since most laboratory INP measurements are performed at relatively high temperatures (Jiang et al., 2016; Reicher et al., 2019; Chen et al., 2021), the reversed trend below –20°C highlights the need for additional measurements at lower temperatures. Reduced INP concentrations in the 0°C to –20°C range weakened the WBF process in Reicher2019, leading to higher liquid water content relative to Chen2021.

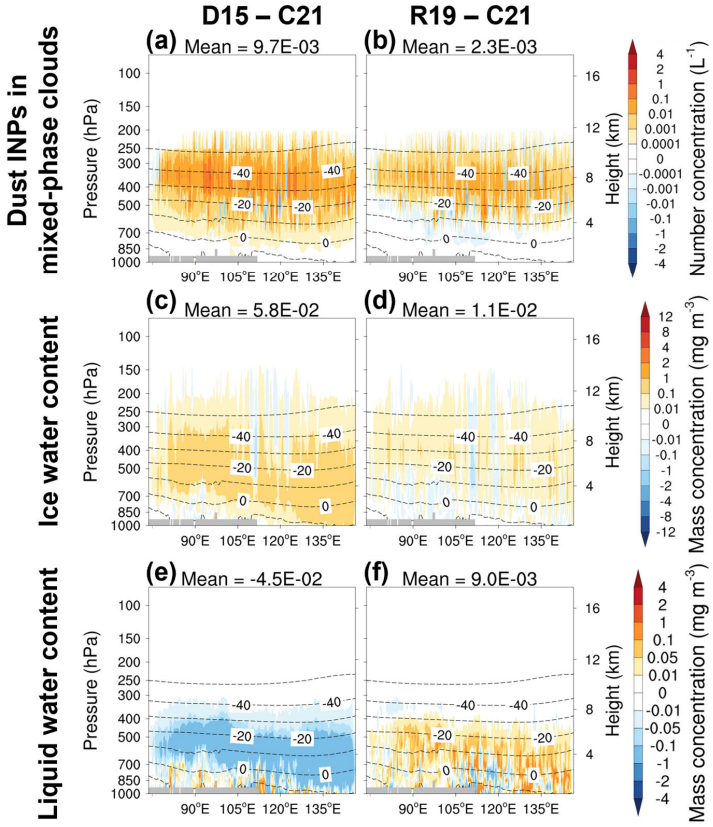

Figure 8. Simulated meridional mean vertical cross-sections of **(a–b)** dust INPs in mixed-phase clouds, **(c–d)** ice water content, and **(e–f)** liquid water content. The left column shows differences between the MixINPs_DeMott2015 scenario (DeMott2015, D15) and the MixINPs scenario (Chen2021, C21), and the right column shows differences between the MixINPs_Reicher2019 scenario (Reicher2019, R19) and the MixINPs scenario (Chen2021, C21). Dashed lines indicate isotherms, and grey shading denotes missing values due to terrain. The mean value over the plotted region is shown above each panel. The simulated results are averages of hourly values from March to May 2018.

The horizontal distribution differences for the same sets of simulations are

https://doi.org/10.5194/egusphere-2025-5277
Preprint. Discussion started: 18 November 2025

presented in Fig. 9. Consistent with the vertical sections, DeMott2015 produced higher INP concentrations, higher ice water path, and lower liquid water path than Chen2021, reaffirming enhanced ice formation through the WBF process. These differences ultimately resulted in a net top-of-atmosphere radiative forcing difference of 0.18 W m^{-2} between DeMott2015 and Chen2021, comparable to the forcing difference between Chen2021 and the NoINPs scenario (MixINPs – NoINPs; Fig. 7g; 0.2 W m^{-2}). Larger differences in INPs, cloud water paths, and radiative effects were found downwind of dust source regions (e.g., from eastern China to Japan), indicating that non-size-resolved parameterizations such as DeMott2015 may overestimate the ice-nucleating ability of finer dust particles and hence their downwind impacts. In contrast, the opposing tendencies in Reicher2019 at temperatures above and below –20°C largely offset each other, resulting in minimal net impacts on clouds and radiation.

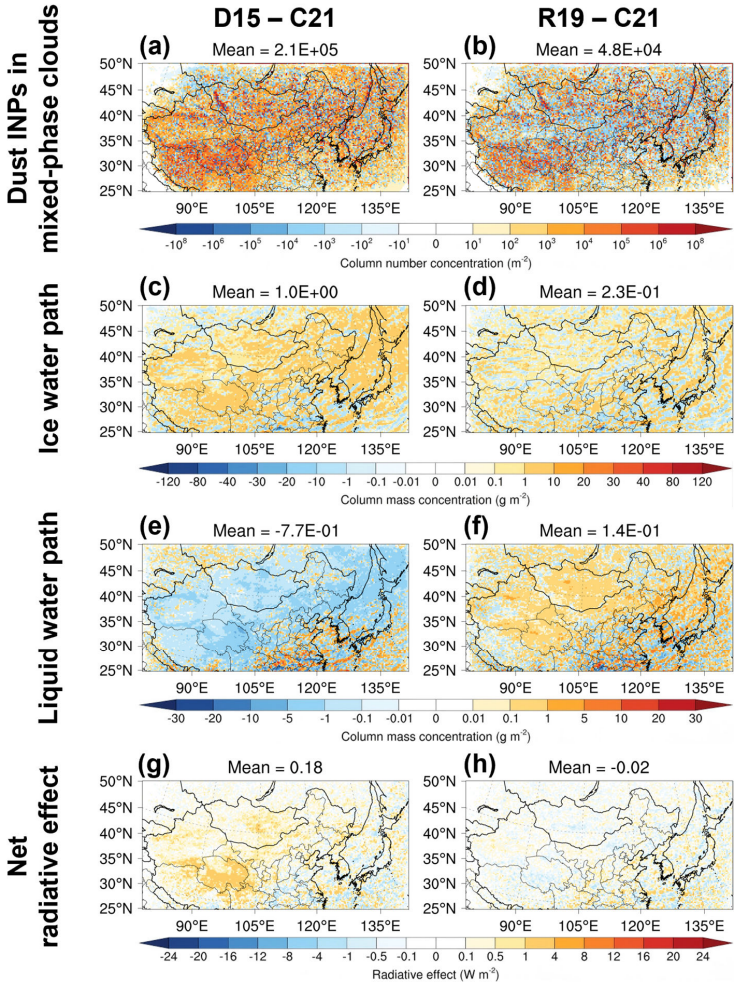

Figure 9. Simulated spatial distributions of **(a–b)** dust INP column number concentrations (vertically

https://doi.org/10.5194/egusphere-2025-5277
Preprint. Discussion started: 18 November 2025

integrated) in mixed-phase clouds, **(c–d)** ice water path, **(e–f)** liquid water path, and **(g-h)** net radiative effect at the top of the atmosphere. The left column shows differences between the MixINPs_DeMott2015 scenario (DeMott2015, D15) and the MixINPs scenario (Chen2021, C21), and the right column shows differences between the MixINPs_Reicher2019 scenario (Reicher2019, R19) and the MixINPs scenario (Chen2021, C21). The mean value over the plotted region is shown above each panel. The simulated results are averages of hourly values from March to May 2018.

4 Conclusions

To investigate how dust ice-nucleating particles (INPs) in mixed-phase and ice clouds modulate cloud microphysical processes and radiative effects, we conducted WRF-Chem simulations over East Asia during spring 2018, using a newly developed dust INP parameterization that explicitly accounts for dust INPs in mixed-phase and ice clouds. Three aerosol-aware parameterizations for dust INPs in mixed-phase clouds were evaluated. Among them, the widely used, non-size-resolved DeMott et al. (2015) scheme predicts INP concentrations about one order of magnitude higher than the size-resolved Chen et al. (2021) scheme at a typical urban site affected by East Asian dust transport, likely due to an overrepresentation of the ice-forming efficiency of smaller dust particles (< 3.2 μm). For ice clouds, the Barahona and Nenes (2009) parameterization provided predictions consistent with available observations.

Our results indicate that dust INPs in mixed-phase clouds trigger ice formation, thereby accelerating the WBF process and enhancing the conversion of hydrometeors from liquid to ice phase. This process increases the number and effective radius of ice crystals, while decreasing the number concentration of cloud droplets and slightly increasing their mean effective radius. Consequently, the IWP increases by 2.3% while the LWP decreases by 3.3%. These microphysical changes lead to a reduction in cloud albedo, allowing more shortwave radiation to enter the atmosphere (0.35 W m^{-2}) and more longwave radiation to escape (0.15 W m^{-2}), resulting in a net radiation increase of 0.20 W m^{-2}.

Dust INPs in ice clouds substantially enhance heterogeneous nucleation, producing approximately 22 times more ice crystals than homogeneous nucleation in the absence of INPs. The presence of dust INP increases the number concentration of ice particles but reduces their effective radius within ice clouds. Sedimentation of ice particles from ice clouds into underlying mixed-phase clouds further accelerates the WBF process, leading to an increase in number and effective radius of ice particles, a reduction in cloud droplet number concentration, and a slight enlargement of droplet mean effective radius. Overall, the IWP increases by 29.1% whereas the LWP decreases by 9.5%. This pronounced enhancement of ice cloud development strengthens both the shortwave reflection to space (5.73 W m^{-2}) and longwave radiation back to the surface (9.29 W m^{-2}). As the longwave effect dominates, the net radiative flux increases by 3.56 W m^{-2}, indicating a notable warming effect. The overall impacts of dust INPs in mixed-

https://doi.org/10.5194/egusphere-2025-5277
Preprint. Discussion started: 18 November 2025

phase and ice clouds on cloud properties and radiation are summarized in Fig. 10.

Our results demonstrate that the variability among mixed-phase cloud INP parameterizations is comparable to the difference between simulations with and without INPs, highlighting the need for further evaluation to constrain inter-scheme uncertainties. The widely used non-size-resolved DeMott et al. (2015) scheme tends to overestimate the ice-nucleating efficiency of fine dust particles, potentially exaggerating the downwind impacts of dust INPs on cloud properties and radiation. In addition, the reversed trends among schemes at temperatures below –20°C underscore the importance of extending INP measurements to colder conditions, thereby enabling the development of parameterizations applicable across a broader temperature range.

This study elucidates the distinct effects of dust INPs in the mixed-phase and ice clouds on cloud microphysical properties and radiation, highlighting the underlying microphysical mechanisms. These finding advance our understanding of aerosol–cloud–climate interactions and provide a foundation for improving the accuracy of climate model projections.

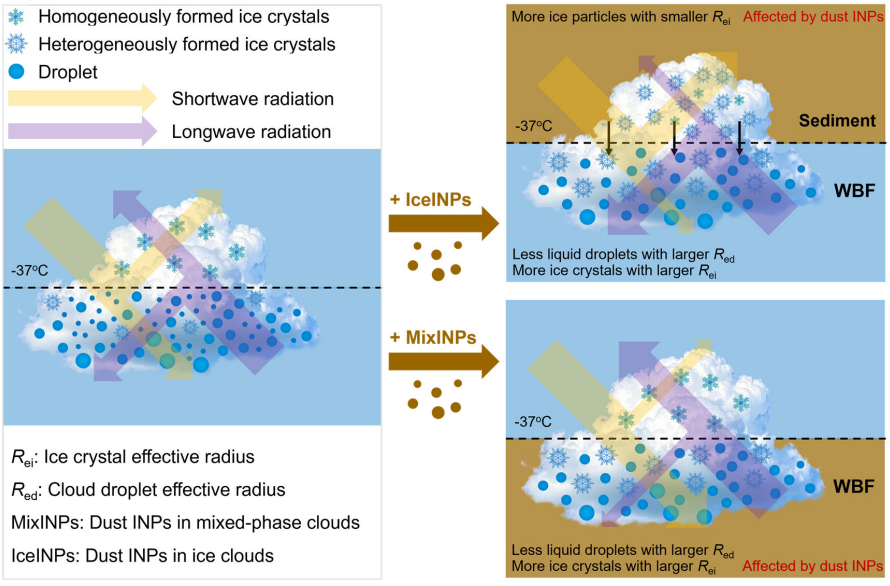

Figure 10. Schematic of the effects of dust INPs in mixed-phase and ice clouds on clouds and radiation. Dust INPs in mixed-phase clouds enhance the Wegener–Bergeron–Findeisen (WBF) process, producing fewer but larger droplets and more, larger ice crystals, which reduce shortwave albedo, increase longwave transmittance, and lead to a net warming effect. In ice clouds, dust INPs intensify heterogeneous nucleation, generating more but smaller ice crystals; their sedimentation further enhances the WBF process in mixed-phase clouds. The much stronger changes in ice clouds amplify the warming effect, dominated by longwave radiation, resulting in an overall net warming.

Code and data availability. The data and code used in this study are available upon

https://doi.org/10.5194/egusphere-2025-5277
Preprint. Discussion started: 18 November 2025

request from the corresponding author.

Author contributions. HZ and BZ designed the research; HZ, BZ, JS, DG, DY, YH, XZ, and SC improved the WRF-Chem performance; HZ and BZ performed the WRF-Chem simulations; JC and HJ processed the observed data of ice-nucleating particles and aerosol number size distribution; SL and ZD processed the anthropogenic emissions; HZ analyzed the data with help from BZ and XZ; ZL helped to design some figures; SW, ZW, YY, DL, and MS presented important suggestions for the analysis and writings; HZ and BZ wrote the paper with input from all the co-authors.

Competing interests. At least one of the (co-)authors is a member of the editorial board of Atmospheric Chemistry and Physics. The authors have no other competing interests to declare.

Acknowledgements. This study was funded by National Key R&D Program of China (2022YFC3701000, Task 5). It is also supported by the Center of High Performance Computing, Tsinghua University. Manish Shrivastava acknowledges support from the US Department of Energy (DOE) Biological and Environmental Research (BER) through its Atmospheric System Research (ASR) program. The Pacific Northwest National Laboratory is operated by Battelle Memorial Institute for the US DOE under Contract DE-AC05-76RL01830.

Reference

Barahona, D. and Nenes, A.: Parameterizing the competition between homogeneous and heterogeneous freezing in ice cloud formation – polydisperse ice nuclei, Atmos. Chem. Phys., 9, 5933–5948, https://doi.org/10.5194/acp-9-5933-2009, 2009.

Beer, C. G., Hendricks, J., and Righi, M.: Impacts of ice-nucleating particles on cirrus clouds and radiation derived from global model simulations with MADE3 in EMAC, Atmos. Chem. Phys., 24, 3217–3240, https://doi.org/10.5194/acp-24-3217-2024, 2024.

Bi, Y., Cao, B., and Li, T.: Enhanced heterogeneous ice nucleation by special surface geometry, Nat. Commun., 8, 15372, https://doi.org/10.1038/ncomms15372, 2017.

Bigg, E. K.: The formation of atmospheric ice crystals by the freezing of droplets, Q. J. R. Meteorolog. Soc., 79, 510–519, https://doi.org/10.1002/qj.49707934207, 1953.

Boose, Y., Sierau, B., García, M. I., Rodríguez, S., Alastuey, A., Linke, C., Schnaiter, M., Kupiszewski, P., Kanji, Z. A., and Lohmann, U.: Ice nucleating particles in the Saharan Air Layer, Atmos. Chem. Phys., 16, 9067–9087, https://doi.org/10.5194/acp-16-9067-2016, 2016.

Burrows, S. M., McCluskey, C. S., Cornwell, G., Steinke, I., Zhang, K., Zhao, B., Zawadowicz, M., Raman, A., Kulkarni, G., China, S., Zelenyuk, A., and DeMott, P. J.: Ice-nucleating particles that impact clouds and climate: Observational and

https://doi.org/10.5194/egusphere-2025-5277
Preprint. Discussion started: 18 November 2025

modeling research needs, Reviews of Geophysics, 60, e2021RG000745, https://doi.org/10.1029/2021RG000745, 2022.

Cantrell, W. and Heymsfield, A.: Production of ice in tropospheric clouds: A review, Bull. Am. Meteorol. Soc., 86, 795–808, https://doi.org/10.1175/BAMS-86-6-795, 2005.

Carter, W.: Documentation of the SAPRC-99 Chemical Mechanism for VOC Reactivity Assessment, Final Report to California Air Resources Board, 2000.

Chen, F. and Mitchell, K.: Using the GEWEX-ISLSCP forcing data to simulate global soil moisture fields and hydrological cycle for 1987-1988, J. Meteorol. Soc. Jpn., II, 77, 167–182, https://doi.org/10.2151/jmsj1965.77.1B_167, 1999.

Chen, J., Wu, Z., Chen, J., Reicher, N., Fang, X., Rudich, Y., and Hu, M.: Size-resolved atmospheric ice-nucleating particles during East Asian dust events, Atmos. Chem. Phys., 21, 3491–3506, https://doi.org/10.5194/acp-21-3491-2021, 2021.

Cooper, W. A.: Ice initiation in natural clouds, in: Precipitation Enhancement—A Scientific Challenge, American Meteorological Society, Boston, MA, 29–32, https://doi.org/10.1007/978-1-935704-17-1_4, 1986.

DeMott, P. J., Prenni, A. J., Liu, X., Kreidenweis, S. M., Petters, M. D., Twohy, C. H., Richardson, M. S., Eidhammer, T., and Rogers, D. C.: Predicting global atmospheric ice nuclei distributions and their impacts on climate, Proc. Natl. Acad. Sci., 107, 11217–11222, https://doi.org/10.1073/pnas.0910818107, 2010.

DeMott, P. J., Prenni, A. J., McMeeking, G. R., Sullivan, R. C., Petters, M. D., Tobo, Y., Niemand, M., Möhler, O., Snider, J. R., Wang, Z., and Kreidenweis, S. M.: Integrating laboratory and field data to quantify the immersion freezing ice nucleation activity of mineral dust particles, Atmos. Chem. Phys., 15, 393–409, https://doi.org/10.5194/acp-15-393-2015, 2015.

Gao, M., Han, Z., Tao, Z., Li, J., Kang, J.-E., Huang, K., Dong, X., Zhuang, B., Li, S., Ge, B., Wu, Q., Lee, H.-J., Kim, C.-H., Fu, J. S., Wang, T., Chin, M., Li, M., Woo, J.-H., Zhang, Q., Cheng, Y., Wang, Z., and Carmichael, G. R.: Air quality and climate change, topic 3 of the model inter-comparison study for Asia phase III (MICS-asia III) – part 2: aerosol radiative effects and aerosol feedbacks, Atmos. Chem. Phys., 20, 1147–1161, https://doi.org/10.5194/acp-20-1147-2020, 2020.

Grell, G. A. and Freitas, S. R.: A scale and aerosol aware stochastic convective parameterization for weather and air quality modeling, Atmos. Chem. Phys., 14, 5233–5250, https://doi.org/10.5194/acp-14-5233-2014, 2014.

Grell, G. A., Peckham, S. E., Schmitz, R., McKeen, S. A., Frost, G., Skamarock, W. C., and Eder, B.: Fully coupled "online" chemistry within the WRF model, Atmos. Environ., 39, 6957–6975, https://doi.org/10.1016/j.atmosenv.2005.04.027, 2005.

Gultepe, I. and Heymsfield, A. J.: Introduction ice fog, ice clouds, and remote sensing, Pure Appl. Geophys., 173, 2977–2982, https://doi.org/10.1007/s00024-016-1380-2, 2016.

Hoinka, K. P.: Statistics of the Global Tropopause Pressure, Mon. Weather Rev., 126, 3303–3325, https://doi.org/10.1175/1520-

https://doi.org/10.5194/egusphere-2025-5277
Preprint. Discussion started: 18 November 2025

0493(1998)126%253C3303:SOTGTP%253E2.0.CO;2, 1998.

Holden, M. A., Whale, T. F., Tarn, M. D., O'Sullivan, D., Walshaw, R. D., Murray, B. J., Meldrum, F. C., and Christenson, H. K.: High-speed imaging of ice nucleation in water proves the existence of active sites, Sci. Adv., 5, eaav4316, https://doi.org/10.1126/sciadv.aav4316, 2019.

Hong, S.-Y., Noh, Y., and Dudhia, J.: A new vertical diffusion package with an explicit treatment of entrainment processes, Mon. Weather Rev., 134, 2318–2341, https://doi.org/10.1175/MWR3199.1, 2006.

Hoose, C., Lohmann, U., Erdin, R., and Tegen, I.: The global influence of dust mineralogical composition on heterogeneous ice nucleation in mixed-phase clouds, Environ. Res. Lett., 3, 025003, https://doi.org/10.1088/1748-9326/3/2/025003, 2008.

Hu, Y., Wang, G., Wei, X., Zhou, F., Kattel, G., Amankwah, S. O. Y., Hagan, D. F. T., and Duan, Z.: Reconstructing long-term global satellite-based soil moisture data using deep learning method, Front. Earth Sci., 11, 1130853, https://doi.org/10.3389/feart.2023.1130853, 2023.

Iacono, M. J., Delamere, J. S., Mlawer, E. J., Shephard, M. W., Clough, S. A., and Collins, W. D.: Radiative forcing by long-lived greenhouse gases: Calculations with the AER radiative transfer models, J. Geophys. Res.: Atmos., 113, 2008JD009944, https://doi.org/10.1029/2008JD009944, 2008.

Jiang, H., Yin, Y., Wang, X., Gao, R., Yuan, L., Chen, K., and Shan, Y.: The measurement and parameterization of ice nucleating particles in different backgrounds of China, Atmos. Res., 181, 72–80, https://doi.org/10.1016/j.atmosres.2016.06.013, 2016.

Jiménez, P. A., Dudhia, J., González-Rouco, J. F., Navarro, J., Montávez, J. P., and García-Bustamante, E.: A revised scheme for the WRF surface layer formulation, Mon. Weather Rev., 140, 898–918, https://doi.org/10.1175/MWR-D-11-00056.1, 2012.

Kanji, Z. A., Ladino, L. A., Wex, H., Boose, Y., Burkert-Kohn, M., Cziczo, D. J., and Krämer, M.: Overview of ice nucleating particles, Meteorol. Monogr., 58, 1.1-1.33, https://doi.org/10.1175/AMSMONOGRAPHS-D-16-0006.1, 2017.

Kawai, K., Matsui, H., and Tobo, Y.: High potential of asian dust to act as ice nucleating particles in mixed-phase clouds simulated with a global aerosol-climate model, JGR Atmospheres, 126, e2020JD034263, https://doi.org/10.1029/2020JD034263, 2021.

Kiselev, A., Bachmann, F., Pedevilla, P., Cox, S. J., Michaelides, A., Gerthsen, D., and Leisner, T.: Active sites in heterogeneous ice nucleation—the example of K-rich feldspars, Science, 355, 367–371, https://doi.org/10.1126/science.aai8034, 2017.

Knopf, D. A., Alpert, P. A., and Wang, B.: The role of organic aerosol in atmospheric ice nucleation: A review, ACS Earth Space Chem., 2, 168–202, https://doi.org/10.1021/acsearthspacechem.7b00120, 2018.

Koop, T., Luo, B., Tsias, A., and Peter, T.: Water activity as the determinant for

https://doi.org/10.5194/egusphere-2025-5277
Preprint. Discussion started: 18 November 2025

homogeneous ice nucleation in aqueous solutions, Nature, 406, 611–614, https://doi.org/10.1038/35020537, 2000.

Kuebbeler, M., Lohmann, U., Hendricks, J., and Kärcher, B.: Dust ice nuclei effects on cirrus clouds, Atmos. Chem. Phys., 14, 3027–3046, https://doi.org/10.5194/acp-14-3027-2014, 2014.

Li, S., Wang, S., Wu, Q., Zhang, Y., Ouyang, D., Zheng, H., Han, L., Qiu, X., Wen, Y., Liu, M., Jiang, Y., Yin, D., Liu, K., Zhao, B., Zhang, S., Wu, Y., and Hao, J.: Emission trends of air pollutants and CO2 in China from 2005 to 2021, Earth Syst. Sci. Data, 15, 2279–2294, https://doi.org/10.5194/essd-15-2279-2023, 2023.

Liu, X. and Penner, J. E.: Ice nucleation parameterization for global models, Meteorol. Z., 14, 499–514, https://doi.org/10.1127/0941-2948/2005/0059, 2005.

Liu, X., Xie, S., Boyle, J., Klein, S. A., Shi, X., Wang, Z., Lin, W., Ghan, S. J., Earle, M., Liu, P. S. K., and Zelenyuk, A.: Testing cloud microphysics parameterizations in NCAR CAM5 with ISDAC and M-PACE observations, J. Geophys. Res., 116, D00T11, https://doi.org/10.1029/2011JD015889, 2011.

Liu, X., Shi, X., Zhang, K., Jensen, E. J., Gettelman, A., Barahona, D., Nenes, A., and Lawson, P.: Sensitivity studies of dust ice nuclei effect on cirrus clouds with the Community Atmosphere Model CAM5, Atmos. Chem. Phys., 12, 12061–12079, https://doi.org/10.5194/acp-12-12061-2012, 2012.

Luo, R., Liu, Y., Luo, M., Li, D., Tan, Z., Shao, T., and Alam, K.: Dust effects on mixed-phase clouds and precipitation during a super dust storm over northern China, Atmos. Environ., 313, 120081, https://doi.org/10.1016/j.atmosenv.2023.120081, 2023.

Meyers, M. P., DeMott, P. J., and Cotton, W. R.: New primary ice-nucleation parameterizations in an explicit cloud model, J. Appl. Meteorol., 31, 708–721, https://doi.org/10.1175/1520-0450(1992)031%253C0708:NPINPI%253E2.0.CO;2, 1992.

Morrison, H., Curry, J. A., and Khvorostyanov, V. I.: A new double-moment microphysics parameterization for application in cloud and climate models. Part I: Description, J. Atmos. Sci., 62, 1665–1677, https://doi.org/10.1175/JAS3446.1, 2005.

Murphy, D. M. and Koop, T.: Review of the vapor pressures of ice and supercooled water for atmospheric applications, Q. J. R. Meteorolog. Soc., 131, 1539–1565, https://doi.org/10.1256/qj.04.94, 2005.

Murray, B. J., O'Sullivan, D., Atkinson, J. D., and Webb, M. E.: Ice nucleation by particles immersed in supercooled cloud droplets, Chem. Soc. Rev., 41, 6519, https://doi.org/10.1039/c2cs35200a, 2012.

Niemand, M., Möhler, O., Vogel, B., Vogel, H., Hoose, C., Connolly, P., Klein, H., Bingemer, H., DeMott, P., Skrotzki, J., and Leisner, T.: A particle-surface-area-based parameterization of immersion freezing on desert dust particles, J. Atmos. Sci., 69, 3077–3092, https://doi.org/10.1175/JAS-D-11-0249.1, 2012.

Phillips, V. T. J., Donner, L. J., and Garner, S. T.: Nucleation processes in deep

https://doi.org/10.5194/egusphere-2025-5277
Preprint. Discussion started: 18 November 2025

convection simulated by a cloud-system-resolving model with double-moment bulk microphysics, J. Atmos. Sci., 64, 738–761, https://doi.org/10.1175/JAS3869.1, 2007.

Phillips, V. T. J., DeMott, P. J., and Andronache, C.: An empirical parameterization of heterogeneous ice nucleation for multiple chemical species of aerosol, J. Atmos. Sci., 65, 2757–2783, https://doi.org/10.1175/2007JAS2546.1, 2008.

Price, H. C., Baustian, K. J., McQuaid, J. B., Blyth, A., Bower, K. N., Choularton, T., Cotton, R. J., Cui, Z., Field, P. R., Gallagher, M., Hawker, R., Merrington, A., Miltenberger, A., Neely Iii, R. R., Parker, S. T., Rosenberg, P. D., Taylor, J. W., Trembath, J., Vergara-Temprado, J., Whale, T. F., Wilson, T. W., Young, G., and Murray, B. J.: Atmospheric ice-nucleating particles in the dusty tropical Atlantic, J. Geophys. Res.: Atmos., 123, 2175–2193, https://doi.org/10.1002/2017JD027560, 2018.

Reicher, N., Budke, C., Eickhoff, L., Raveh-Rubin, S., Kaplan-Ashiri, I., Koop, T., and Rudich, Y.: Size-dependent ice nucleation by airborne particles during dust events in the Eastern Mediterranean, Atmos. Chem. Phys., 19, 11143–11158, https://doi.org/10.5194/acp-19-11143-2019, 2019.

Seinfeld, J. H., Bretherton, C., Carslaw, K. S., Coe, H., DeMott, P. J., Dunlea, E. J., Feingold, G., Ghan, S., Guenther, A. B., Kahn, R., Kraucunas, I., Kreidenweis, S. M., Molina, M. J., Nenes, A., Penner, J. E., Prather, K. A., Ramanathan, V., Ramaswamy, V., Rasch, P. J., Ravishankara, A. R., Rosenfeld, D., Stephens, G., and Wood, R.: Improving our fundamental understanding of the role of aerosol−cloud interactions in the climate system, Proc. Natl. Acad. Sci., 113, 5781–5790, https://doi.org/10.1073/pnas.1514043113, 2016.

Shao, Y., Ishizuka, M., Mikami, M., and Leys, J. F.: Parameterization of size-resolved dust emission and validation with measurements, J. Geophys. Res., 116, D08203, https://doi.org/10.1029/2010JD014527, 2011.

Shi, X., Liu, X., and Zhang, K.: Effects of pre-existing ice crystals on cirrus clouds and comparison between different ice nucleation parameterizations with the community atmosphere model (CAM5), Atmos. Chem. Phys., 15, 1503–1520, https://doi.org/10.5194/acp-15-1503-2015, 2015.

Shi, Y. and Liu, X.: Dust radiative effects on climate by glaciating mixed-phase clouds, Geophys. Res. Lett., 46, 6128–6137, https://doi.org/10.1029/2019GL082504, 2019.

Shi, Y., Liu, X., Wu, M., Zhao, X., Ke, Z., and Brown, H.: Relative importance of high-latitude local and long-range-transported dust for Arctic ice-nucleating particles and impacts on Arctic mixed-phase clouds, Atmos. Chem. Phys., 22, 2909–2935, https://doi.org/10.5194/acp-22-2909-2022, 2022.

Su, L. and Fung, J. C. H.: Investigating the role of dust in ice nucleation within clouds and further effects on the regional weather system over East Asia – Part 1: Model development and validation, Atmos. Chem. Phys., 18, 8707–8725, https://doi.org/10.5194/acp-18-8707-2018, 2018a.

https://doi.org/10.5194/egusphere-2025-5277
Preprint. Discussion started: 18 November 2025

Su, L. and Fung, J. C. H.: Investigating the role of dust in ice nucleation within clouds and further effects on the regional weather system over East Asia – Part 2: modification of the weather system, Atmos. Chem. Phys., 18, 11529–11545, https://doi.org/10.5194/acp-18-11529-2018, 2018b.

Sun, J., Zhang, M., and Liu, T.: Spatial and temporal characteristics of dust storms in China and its surrounding regions, 1960–1999: Relations to source area and climate, J. Geophys. Res.: Atmos., 106, 10325–10333, https://doi.org/10.1029/2000JD900665, 2001.

Tewari, M., Chen, F., Wang, W., Dudhia, J., LeMone, M. A., Mitchell, K., Ek, M., Gayno, G., Wegiel, J., and Cuenca, R. H.: Implementation and verification of the unified noah land surface model in the WRF model, Bull. Am. Meteorol. Soc., 2165–2170, 2004.

Textor, C., Schulz, M., Guibert, S., Kinne, S., Balkanski, Y., Bauer, S., Berntsen, T., Berglen, T., Boucher, O., Chin, M., Dentener, F., Diehl, T., Easter, R., Feichter, H., Fillmore, D., Ghan, S., Ginoux, P., Gong, S., Grini, A., Hendricks, J., Horowitz, L., Huang, P., Isaksen, I., Iversen, I., Kloster, S., Koch, D., Kirkevåg, A., Kristjansson, J. E., Krol, M., Lauer, A., Lamarque, J. F., Liu, X., Montanaro, V., Myhre, G., Penner, J., Pitari, G., Reddy, S., Seland, Ø., Stier, P., Takemura, T., and Tie, X.: Analysis and quantification of the diversities of aerosol life cycles within AeroCom, Atmos. Chem. Phys., 6, 1777–1813, https://doi.org/10.5194/acp-6-1777-2006, 2006.

Twomey, S.: Pollution and the planetary albedo, Atmos. Environ. (1967), 8, 1251–1256, https://doi.org/10.1016/0004-6981(74)90004-3, 1974.

Vali, G.: Nucleation terminology, Bull. Am. Meteorol. Soc., 66, 1426–1427, 1985.

Wang, J., Xu, X., Henze, D. K., Zeng, J., Ji, Q., Tsay, S., and Huang, J.: Top-down estimate of dust emissions through integration of MODIS and MISR aerosol retrievals with the GEOS-Chem adjoint model, Geophys. Res. Lett., 39, 2012GL051136, https://doi.org/10.1029/2012GL051136, 2012.

Weger, M., Heinold, B., Engler, C., Schumann, U., Seifert, A., Fößig, R., Voigt, C., Baars, H., Blahak, U., Borrmann, S., Hoose, C., Kaufmann, S., Krämer, M., Seifert, P., Senf, F., Schneider, J., and Tegen, I.: The impact of mineral dust on cloud formation during the Saharan dust event in April 2014 over Europe, Atmos. Chem. Phys., 18, 17545–17572, https://doi.org/10.5194/acp-18-17545-2018, 2018.

Zaveri, R. A., Easter, R. C., Fast, J. D., and Peters, L. K.: Model for Simulating Aerosol Interactions and Chemistry (MOSAIC), J. Geophys. Res.: Atmos., 113, 2007JD008782, https://doi.org/10.1029/2007JD008782, 2008.

Zeng, Y., Wang, M., Zhao, C., Chen, S., Liu, Z., Huang, X., and Gao, Y.: WRF-Chem v3.9 simulations of the East Asian dust storm in May 2017: modeling sensitivities to dust emission and dry deposition schemes, Geosci. Model Dev., 13, 2125–2147, https://doi.org/10.5194/gmd-13-2125-2020, 2020.

Zeng, Y., Wang, M., Zhao, C., Zhu, Y., Rosenfeld, D., and Huang, K.: Extremely High Concentrations of Ice Particles in East Asian Dust-Infused Baroclinic Storm

https://doi.org/10.5194/egusphere-2025-5277
Preprint. Discussion started: 18 November 2025

(DIBS) Cirrus Shield: Dominant Role of Dust Ice Nucleation Effect, J. Geophys. Res.: Atmos., 128, e2022JD038034, https://doi.org/10.1029/2022JD038034, 2023.

Zhang, B., Tsunekawa, A., and Tsubo, M.: Contributions of sandy lands and stony deserts to long-distance dust emission in China and Mongolia during 2000–2006, Global Planet. Change, 60, 487–504, https://doi.org/10.1016/j.gloplacha.2007.06.001, 2008.

Zhang, L.: A size-segregated particle dry deposition scheme for an atmospheric aerosol module, Atmos. Environ., 35, 549–560, https://doi.org/10.1016/S1352-2310(00)00326-5, 2001.

Zhao, B., Wang, Y., Gu, Y., Liou, K.-N., Jiang, J. H., Fan, J., Liu, X., Huang, L., and Yung, Y. L.: Ice nucleation by aerosols from anthropogenic pollution, Nat. Geosci., 12, 602–607, https://doi.org/10.1038/s41561-019-0389-4, 2019.

Zheng, H., Cai, S., Wang, S., Zhao, B., Chang, X., and Hao, J.: Development of a unit-based industrial emission inventory in the Beijing–Tianjin–Hebei region and resulting improvement in air quality modeling, Atmos. Chem. Phys., 19, 3447–3462, https://doi.org/10.5194/acp-19-3447-2019, 2019.